



# 1 Mercury records covering the past 90 kyr 2 from lakes Prespa and Ohrid, SE Europe

3 Alice R. Paine<sup>1\*</sup>, Isabel M. Fendley<sup>1</sup>, Joost Frieling<sup>1</sup>, Tamsin A. Mather<sup>1</sup>, Jack H. Lacey<sup>2</sup>, Bernd  
4 Wagner<sup>3</sup>, Stuart A. Robinson<sup>1</sup>, David M. Pyle<sup>1</sup>, Alexander Francke<sup>4</sup>, Theodore R Them II<sup>5</sup>,  
5 Konstantinos Panagiotopoulos<sup>3</sup>

6 <sup>1</sup>Department of Earth Sciences, University of Oxford, UK, OX1 3AN

7 <sup>2</sup>National Environmental Isotope Facility, British Geological Survey, Nottingham, UK

8 <sup>3</sup>Institute of Geology and Mineralogy, University of Cologne, Cologne, Germany

9 <sup>4</sup>Department of Archeology, College of Humanities, Arts and Social Sciences, Flinders University, Adelaide, 5001, Australia

10 <sup>5</sup>Department of Geology and Environmental Geosciences, College of Charleston, Charleston, SC 29424, USA

11 \*Corresponding Author: [alice.paine@earth.ox.ac.uk](mailto:alice.paine@earth.ox.ac.uk)

12

## 13 ABSTRACT

14 The element mercury (Hg) is a key pollutant, and much insight has been gained by studying the present-day  
15 Hg cycle. However, many important processes within this cycle operate on timescales responsive to  
16 centennial to millennial-scale environmental variability, highlighting the importance of also investigating the  
17 longer-term Hg records in sedimentary archives. To this end, we here explore the timing, magnitude, and  
18 expression of Hg signals retained in sediments over the past ~90 ka from two lakes, linked by a  
19 subterranean karst system: Lake Prespa (Greece/North Macedonia/Albania) and Lake Ohrid (North  
20 Macedonia/Albania). Results suggest that Hg fluctuates largely independent of variability in common host  
21 phases in each lake, and the recorded sedimentary Hg signals show distinct differences first during the late  
22 Pleistocene (Marine Isotope Stages 2-5). The Hg signals in Lake Prespa sediments highlights an abrupt,  
23 short-lived, peak in Hg accumulation coinciding with local deglaciation. In contrast, Lake Ohrid shows a  
24 broader interval with enhanced Hg accumulation, and, superimposed, a series of low-amplitude oscillations  
25 in Hg concentration peaking during the Last Glacial Maximum, that may result from elevated clastic inputs.  
26 Divergent Hg signals are also recorded during the early and middle Holocene (Marine Isotope Stage 1).  
27 Here, Lake Prespa sediments show a series of large Hg peaks; while Lake Ohrid sediments show a  
28 progression to lower Hg values. Around 3 ka, anthropogenic influences overwhelm local fluxes in both lakes.  
29 The lack of coherence in Hg accumulation between the two lakes suggests that, in the absence of an  
30 exceptional perturbation, local differences in sediment composition, lake structure, and water balance all  
31 influence the local Hg cycle, and determine the extent to which Hg signals reflect local or global-scale  
32 environmental changes.

33

## 34 1. Introduction

35 Mercury (Hg) is a volatile metal released into the atmosphere by both natural processes and human  
36 activities. Emission of Hg by geological sources/processes are unevenly distributed across the Earth's



37 surface, and are generally concentrated where tectonic, volcanic, and geothermal activities are most  
38 intense (Rytuba, 2003; Edwards et al., 2021; Schlüter, 2000). Geological processes have been major  
39 drivers of variability in the global Hg cycle throughout Earth's history (Selin, 2009), leading to the use  
40 of sedimentary Hg to reconstruct periods of intense volcanism (e.g., large igneous provinces (LIPs)) in  
41 Earth's geological past (e.g., Grasby et al., 2019; Percival et al., 2018). However, Hg release  
42 associated with industrialisation, the extraction and combustion of fossil fuels, and natural resources  
43 (metals) has overwhelmed the natural background flux (Outridge et al., 2018; Streets et al., 2019;  
44 United Nations Environment Programme, 2018).

45 Existing in the atmosphere primarily in the form of gaseous elemental mercury, Hg has an  
46 atmospheric lifetime of up to 2 years, facilitating its deposition far from the original source (Lyman et  
47 al., 2020). Once removed from the atmosphere, Hg may enter the terrestrial environment where it is  
48 cycled between reservoirs by a complex series of processes, many of which occur on timescales that  
49 exceed present-day monitoring (**Fig. 1**) (Branfireun et al., 2020; Selin, 2009). Aquatic sediments are  
50 particularly effective sinks within the global Hg cycle (Bishop et al., 2020; Selin, 2009). Here, organic  
51 processes lead to the formation of methylmercury (MeHg), which is the most bio-accumulative Hg  
52 species and can cause severe neurological and physiological damage to complex organisms if  
53 ingested (Driscoll et al., 2013; Wang et al., 2019).

54 The ecological and societal risks of environmental Hg contamination underscore the importance of  
55 quantifying how natural and anthropogenic processes may influence Hg sequestration within aquatic  
56 systems, and the timescales upon which they are effective. Time-resolved sediment records sourced  
57 from marine and lacustrine basins are highly suitable for assessing these roles further back in time, as  
58 they can provide time-resolved records of Hg deposition, cycling, burial, and accumulation relative to  
59 changing environmental conditions on a local, regional, even global-scale (Cooke et al., 2020;  
60 Zaferani and Biester, 2021). Therefore, they can offer new insights into the cycling of Hg in the  
61 terrestrial realm.

62 Analysis of pre-industrial marine and lake sediment records suggest that Hg composition broadly  
63 reflects variability in climate (Li et al., 2020). On orbital ( $>10^3$ -year) timescales, oceanic Hg signals  
64 manifest as low-amplitude fluctuations corresponding to global-scale climate shifts from warm  
65 (interglacial) to colder (glacial) conditions; for example due to changes in atmospheric composition  
66 (e.g., mineral dust loading) and circulation, biogeochemical cycling (Figueiredo et al., 2022), and/or  
67 ocean circulation (Figueiredo et al., 2020; Gelety et al., 2007; Jitaru et al., 2009; Kita et al., 2016). On  
68 centennial to millennial ( $10^2$ - $10^3$ -years) timescales, lacustrine Hg signals correspond more closely to  
69 transient changes in hydrology, landscape dynamics, and ice/permafrost extent on local/regional  
70 scales (Chede et al., 2022; Cordeiro et al., 2011; de Lacerda et al., 2017; Fadina et al., 2019; Li et al.,  
71 2023; Pérez-Rodríguez et al., 2018, 2015) (**Fig. 1**). Importantly, climate-associated Hg signals  
72 retained in lacustrine records integrate a range of processes and some records show higher  
73 sedimentary Hg concentrations during cold, arid conditions (e.g., Li et al., 2020), while other records  
74 tend to have higher Hg concentrations with warm and wet climates. For example, increases in  
75 catchment-sourced detrital input have been proposed as the primary cause of Hg enrichment in



76 temperate lakes (Pan et al., 2020; Schütze et al., 2018), and near-shore marine records (Fadina et  
77 al., 2019). Conversely, lakes located in glaciated regions may show dilution of Hg by the same inputs  
78 (Schneider et al., 2020). Local, site-specific factors are therefore likely to influence sedimentary Hg  
79 records. Yet, the combined effects of global and local processes complicate study of how changes in  
80 the terrestrial Hg cycle may translate to measurable sedimentary signals and signals that are  
81 comparable between different regional or global archives.

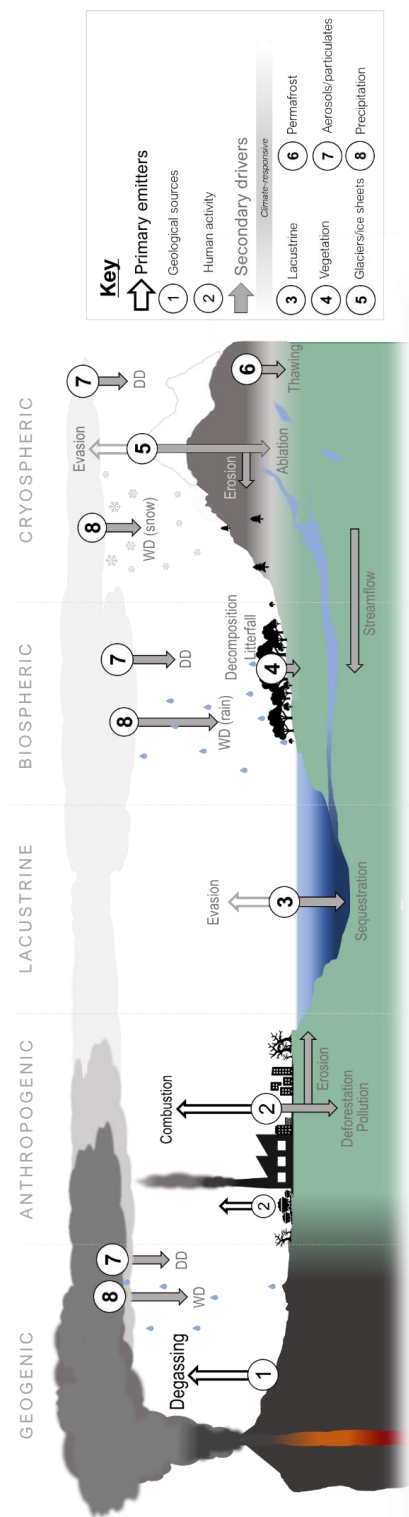


**Figure 1:** A summary diagram depicting the key anthropogenic, geogenic, biospheric, cryospheric, and lacustrine processes, which could generate and modify a sedimentary Hg signal over 10<sup>1</sup>-10<sup>5</sup>-year timescales. Processes are abbreviated as: WD – wet deposition, DD – dry deposition. Non-filled arrows depict processes acting to increase the atmospheric Hg burden, and colour filled arrows depict processes acting to influence the quantity of Hg stored in terrestrial reservoirs. This figure is schematic (not drawn to scale), and constructed on the basis of reviews by Bishop et al. (2020), Obrist et al. (2018), Selin et al. (2009).



### 83 1.1 Sedimentary mercury records

84 Sedimentary Hg concentrations at discrete intervals can be quantified using the total Hg concentration  
85 ( $Hg_T$ ) (Bishop et al., 2020; Kohler et al., 2022; Nasr et al., 2011). However, changes in bioproductivity,  
86 organic matter type and/or flux, sedimentation rate, pH, and redox conditions could all produce a  
87 distinct, local, transient, sedimentary Hg enrichment without a meaningful change in the total amount  
88 of Hg present and/or mobile in the system. In light of these complexities, it has become common  
89 practice to examine total Hg concentration ( $Hg_T$ ) alongside normalized Hg. Normalisation is often  
90 applied when it can be shown that the abundance of a carrier (or “host”) phase directly impacts Hg  
91 content. This impact is then removed, via normalisation (e.g.  $Hg/TOC$ ,  $Hg/TS$ ), to reveal changes in  
92 environmental Hg availability (Grasby et al., 2019; Percival et al., 2015; Shen et al., 2020; Them et al.,  
93 2019). Such an approach is particularly beneficial for studies typically spanning  $>10^2$ -year timescales,  
94 where the goal is to isolate the effects of local depositional and/or transport processes on Hg signals  
95 recorded in the sediment through time.

96 Organic matter (hereafter represented by total organic carbon (TOC)) is generally considered the  
97 dominant carrier phase of sedimentary Hg (Chakraborty et al., 2015; Ravichandran, 2004). For  
98 records in which TOC and Hg co-vary linearly, Hg is generally normalized to TOC (Chede et al., 2022;  
99 Figueiredo et al., 2022a, 2020; Kita et al., 2016a; Outridge et al., 2019). Some systems do not exhibit  
100 a relation to TOC and Hg may instead be adsorbed onto (fine-grained) detrital minerals and detected  
101 by a correlation between Hg and mineral dominating elements such as aluminium (Al), titanium (Ti),  
102 zirconium (Zr), rubidium (Rb), or potassium (K) (Sanei et al., 2012; Sial et al., 2013; Them et al.,  
103 2019). In few cases, sulphide minerals may act as important Hg hosts (Benoit et al., 1999; Han et al.,  
104 2008), however this is less common in freshwater lacustrine systems where sulphate-reduction is  
105 often limited and only a small fraction of non-organic sulfur is buried (Ding et al., 2016; Holmer and  
106 Storkholm, 2001; Tisserand et al., 2022; Watanabe et al., 2004).

107 Mercury’s relationship with other sedimentary components is often complex. For example,  $Hg_T$  may  
108 also be suppressed through dilution by Hg-poor detrital or biogenic (carbonate, silica) material, and  
109 Hg in many sediments is not exclusively or clearly modulated by balances between host-phase  
110 abundance and dilution. Notably, this can also occur when the host-phases are always present in  
111 sufficient quantities to sequester available Hg. In such cases, and where (single) host-phase  
112 abundance or dilution cannot be easily accounted for,  $Hg_{AR}$  may provide the most optimal assessment  
113 of Hg availability through time as long as a robust age model is available for the archive.

114 Sedimentary TOC, total sulphur (TS), and detrital and biogenic mineral concentrations change in  
115 space and time, underscoring the need to assess how Hg covaries in relation to different host phases  
116 and other sedimentary materials. Hydrology, sedimentation regime, and geochemistry may each  
117 influence mercury host-phase availability and burial in a lacustrine system, and are likely to change  
118 through time, highlighting the importance of investigating the longer-term records of Hg burial and  
119 accumulation in sedimentary archives.



120 This study explores the timing, magnitude, and expression of Hg signals retained in the sediment  
121 records of Lake Prespa (Greece/Albania/North Macedonia) and Lake Ohrid (North  
122 Macedonia/Albania) over the past ~90 ka. The two lakes are located only ~10 km apart (**Fig. 2**), are  
123 hydrologically connected by karst aquifers with ~50% of water inflow to Lake Ohrid originating from  
124 Lake Prespa (Matzinger et al., 2006), and their sediments encode records of environmental change in  
125 southeast Europe over the last ~90 ka (Damaschke et al., 2013; Francke et al., 2016; Leng et al.,  
126 2010; Panagiotopoulos et al., 2014; Sadori et al., 2016; Wagner et al., 2010). Comparison of their  
127 sedimentary records provides a rare opportunity to explore three important questions. First, how does  
128 the local sedimentary environment (e.g., host phase availability and sources) influence Hg burial?  
129 Second, do Hg signals reflect changes in catchment hydrology, structure, and/or varying degrees of  
130 interaction between the two lake systems? Finally, could regional-scale climate variability have  
131 measurably affected the Hg signals retained in the sediments?

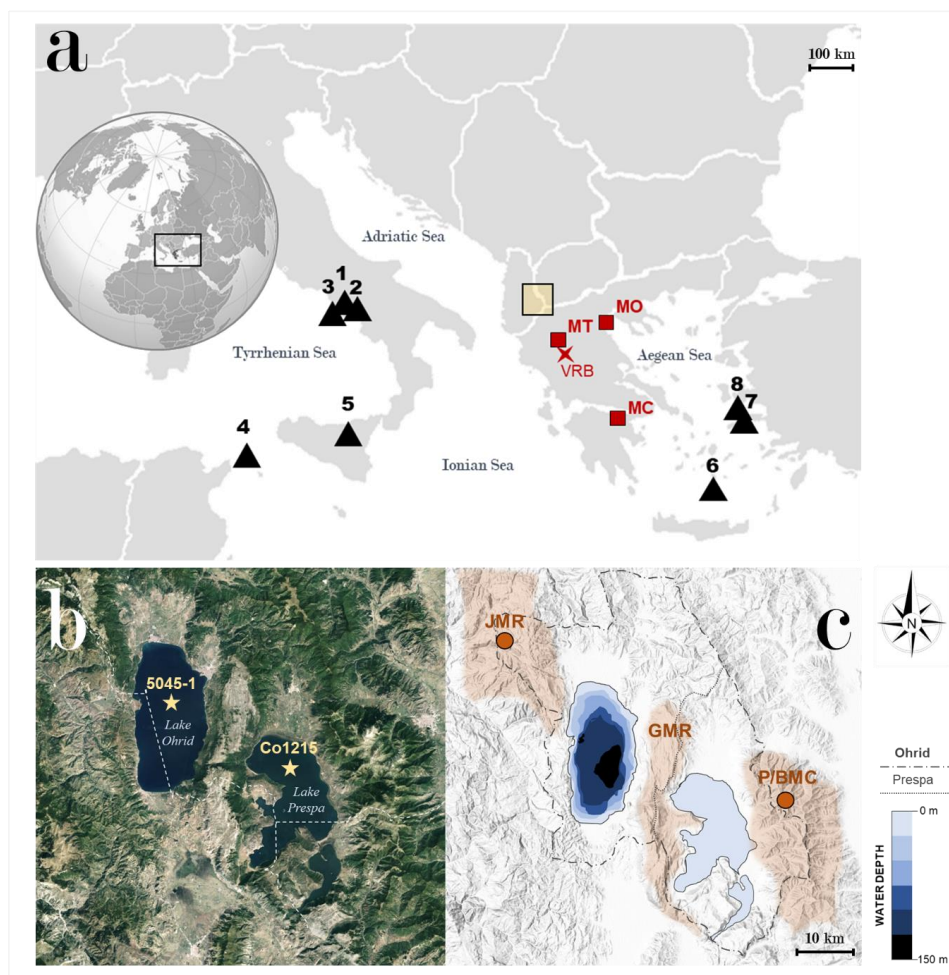


**Figure 2:** (a) Map showing the location of lakes Prespa and Ohrid within Southern Europe (yellow shaded box). Volcanoes from which tephra has been identified in Co1215 (Prespa) and/or 5045-1 (Ohrid) are coloured as black triangles, and numbered as: 1 – Vesuvius, 2 – Campi Flegrei, 3 – Ischia, 4 - Pantelleria, 5 – Etna. Volcanoes of the South Aegean Volcanic Arc with known explosive eruptions (>magnitude 4.0) between 90 and 0 ka are also numbered: 6 – Santorini, 7 – Nisyros, 8 – Yali. Sites referred to in this study are also labelled as follows: (red squares) MT – Mount Tymphi, MO – Mount Olympus, MC – Mount Chelmos; (red star) VRB – Voidomatis river basin. (b) Aerial photo showing the coring locations of Co1215 and 5045-1, and illustrating the vegetation distributions of the area surrounding lakes Prespa and Ohrid. Base image sourced from © GoogleEarth v 9.177.0.1™. (c) Hillshade map of the Prespa/Ohrid region and bathymetric data of lakes Prespa and Ohrid (Jovanovska et al., 2016; Wagner et al., 2022). Grey dashed lines denote watershed boundaries for lakes Prespa and Ohrid, respectively adapted from Panagiotopoulos et al. (2019). Basemap sourced from ArcGIS v 10.0™ (spatial reference 102100 (3857)). Orange shading denotes mountain ranges are labelled as: P/BMC – Pelister/Baba mountain chain (circle marking the location of Mount Pelister: 2601 m a.s.l.), GMR – Galičica mountain range, and JMR – Jablanica mountain range (circle marking the location of Jablanica Mountain - 2257 m a.s.l.). All mountain ranges contain evidence for the presence of glaciers and/or (peri)glacial features of late Pleistocene age (Hughes et al., 2022, 2023)



## 133 2. Site Description

### 134 2.1. Regional Climate

135 The Mediterranean Sea and the European continent are both major influences on present-day climate  
136 of the region surrounding lakes Prespa and Ohrid. Summer months (July to August) are hot and dry  
137 (average monthly air temperature +26 °C) while winter months (November to January) are cold,  
138 cloudy and wet, with an average monthly air temperature of -1 °C (Matzinger et al., 2006). Annual  
139 precipitation in the region averages ~750 mm yr<sup>-1</sup>, with winter precipitation falling predominantly as  
140 snow at high elevations (Hollis and Stevenson, 1997).

141 Present-day vegetation in the Prespa/Ohrid region comprises a mixture of Balkan endemic, central  
142 European, and Mediterranean species (Donders et al., 2021; Panagiotopoulos et al., 2014, 2020;  
143 Sadori et al., 2016). During the last glacial-interglacial cycle (~100-kyr), sedimentary pollen records  
144 from lakes Prespa and Ohrid show three primary stages of vegetation distribution at mid/low altitudes  
145 in the catchment: (1) forested, (2) open with significant presence of deciduous trees, and (3) open  
146 with significant presence of evergreen vegetation (Panagiotopoulos et al., 2014; Sadori et al., 2016).  
147 The timing of shifts in vegetation generally corresponds to the large-scale climate oscillations  
148 captured by terrestrial and marine proxy records across the Northern Hemisphere (e.g., Rasmussen  
149 et al., 2014; Sanchez Goñi and Harrison, 2010; Tzedakis et al., 2006). Warmer and wetter interglacial  
150 conditions generally correspond to a more forested catchment in the Prespa/Ohrid region, and cooler,  
151 drier conditions correspond to a more open catchment.

152 The Balkan Peninsula contains evidence for recurrent glaciation during the late Quaternary (Hughes  
153 et al., 2022). Radiometric dating of moraines, boulders, and outwash sediments indicate that glaciers  
154 present in high-altitude regions reached their peak volume and/or extent between ~40 and 23 ka  
155 (Allard et al., 2021; Hughes and Woodward, 2017; Leontaritis et al., 2020). Evidence for moraine  
156 formation on Mount Pelister (~10 km NE of Lake Prespa) (Ribolini et al., 2018) and Mount Jablanica  
157 (~15 km NW of Lake Ohrid) (Ruszkiczay-Rüdiger et al., 2020) (**Fig. 2**), and identification of glacial tills  
158 and moraine deposits in the Prespa/Ohrid catchment (Belmecheri et al., 2009; Gromig et al., 2018)  
159 provides further evidence that glaciers and (peri)glacial features were present in the catchment during  
160 the late Pleistocene.

161

### 162 2.2. Lake Prespa

163 The Prespa lake system (40°54' N, 21°02' E) is composed of two lakes separated by an isthmus and  
164 located on the tripoint of North Macedonia, Albania and Greece, at an altitude of 844 metres (m) a.s.l.  
165 The ~1300 km<sup>2</sup> catchment of the Prespa lakes encompasses the Pelister Mountains to the east and  
166 the Galičica Mountains to the southwest and west (**Fig. 2**). Here we focus on Megali Prespa  
167 (hereafter referred to as Lake Prespa), the larger of the two lakes, which has a surface area of 254  
168 km<sup>2</sup>, a maximum water depth of 48 m, and a mean water depth of 14 m. The total inflow into Lake  
169 Prespa averages ~16.9 m<sup>3</sup> s<sup>-1</sup> (Matzinger et al., 2006). Water input is sourced from river runoff (56%),



170 direct precipitation (35%), and inflow from the smaller of the two lakes (Mikri Prespa; 9%) (Matzinger  
171 et al., 2006). Lake Prespa has no surface outflow. The residence time of the lake's waters is ~11  
172 years (Matzinger et al., 2006) and water is predominantly lost through evaporation (52%),  
173 underground karst channels into Lake Ohrid located 10 km to the west (46%), and irrigation (2%). The  
174 lake is currently mesotrophic with an average total phosphorus (TP) concentration of 31 mg m<sup>-3</sup> in the  
175 water column, basal anoxia in summer months, and generally clear waters; all signalling moderate  
176 biological productivity (Hollis and Stevenson, 1997). However, the lake likely held a more oligotrophic  
177 (low) nutrient status during the colder late Pleistocene, where biological productivity reduced  
178 substantially (Matzinger et al., 2006; Wagner et al., 2010).

179

### 180 2.3. Lake Ohrid

181 Lake Ohrid (41°02' N, 20°43' E) lies 693 m a.s.l. Separated from Lake Prespa by the Galiçica  
182 Mountains, the lake straddles the boundary between North Macedonia and Albania (**Fig. 2**). The lake  
183 is ~30 km long and 15 km wide, with a maximum water depth of 293 m, water volume of 55.4 km<sup>3</sup>,  
184 and hydraulic residence time of ~70 years. Water input is sourced from direct precipitation (23%),  
185 river inflow (24%), and karst springs (53%) fed by precipitation and water from Lake Prespa  
186 (Matzinger et al., 2006; Lacey and Jones, 2018), and this hydrological link increases the Ohrid  
187 catchment by ~1300 km<sup>2</sup> to ~2610 km<sup>2</sup>. Evaporation (40%) and outflow via the river Crn Drim (60%)  
188 are the dominant pathways for water loss from Lake Ohrid, and complete mixing of the lake occurs  
189 only every few years (Matzinger et al., 2006). The present-day lake shows low levels of biological  
190 productivity (oligotrophic) with an average dissolved phosphorus content of 4.5 mg m<sup>-3</sup>, and regular  
191 mixing maintains moderately oxygenated bottom waters (Matzinger et al., 2006; Wagner et al., 2010).

192

## 193 3. Methods

### 194 3.1. Lake Prespa (Co1215)

195 Composite core Co1215 was recovered in autumn 2009 and summer 2011 from the central-northern  
196 section of Lake Prespa (40°57'50" N, 20°58'41" E, **Fig. 2**). Sediment recovery was performed using a  
197 floating platform, with a gravity corer for surface sediments and a 3-m-long percussion piston corer  
198 (UWITEC Co. Austria) for deeper sediments. Overlapping 3-m-long sediment cores were cut into  
199 segments of up to 1 m in length for transport and storage. After splicing and correlation of core  
200 segments according to geochemical and optical information, the resulting 17.7 m composite core was  
201 continuously sampled at 2-cm-resolution, yielding a total of 849 samples. It is comprised of three  
202 major lithofacies, which differ in colour, sediment structure, grain size, organic-matter and carbonate  
203 content, and geochemistry. There are no lithological indications of any hiatuses or instances of non-  
204 contiguous sedimentation in core Co1215. A detailed lithostratigraphic characterisation of the entire  
205 succession (90–0 ka) is presented in Damaschke et al. (2013), along with details of the six visible  
206 tephra layers and five cryptotephra layers identified in Co1215 (**Table S1**).



207 Published data for Lake Prespa (Co1215) includes: total carbon (TC), total inorganic carbon (TIC),  
208 and total sulphur (TS) analyses (Aufgebauer et al., 2012; Damaschke et al., 2013). These data were  
209 measured at ~2 cm resolution with a DIMATOC 200 (DIMATEC Co., Germany), and TS using a Vario  
210 Micro Cube combustion CNS elemental analyser (VARIO Co.) at the University of Cologne. TOC was  
211 calculated as the difference between TC and TIC (Aufgebauer et al., 2012; Damaschke et al., 2013).  
212 The inorganic chemistry of the sediments was determined by X-ray fluorescence (XRF) data,  
213 generated using an ITRAX core scanner (COX Ltd., Sweden) equipped with a Mo-tube set to 30 kV  
214 and 30 mA, and a Si-drift chamber detector (Wagner et al., 2012). Core Co1215 was scanned with a  
215 resolution of 2 mm and a scanning time of 10 seconds per measurement. Elemental intensities were  
216 obtained for potassium (K), titanium (Ti), manganese (Mn), strontium (Sr), iron (Fe), calcium (Ca), and  
217 rubidium (Rb) (Wagner et al., 2012).  
218

### 219 3.1.1. Chronology

220 A chronology for Co1215 was previously produced by linear interpolation using volcanic ash layers,  
221 coupled with  $^{14}\text{C}$  and electron spin resonance (ESR) dates obtained for bulk organic, fish, and aquatic  
222 plant remains (Aufgebauer et al., 2012). Here, we update this chronology with a Bayesian age-depth  
223 model that re-calculates previously obtained  $^{14}\text{C}$ -dates (**Table S2**) with the latest (Intcal2020)  
224 radiocarbon calibration (**Fig. 3**) (Reimer et al., 2020). We used rBacon v 2.5.7 (Blaauw and Christen,  
225 2011), and the new age model includes updated  $^{40}\text{Ar}/^{39}\text{Ar}$  dates of two eruptions geochemically  
226 correlated to specific tephra layers within the Prespa core (Damaschke et al., 2013); the Y-5 ( $39.85 \pm$   
227  $0.14$  ka (Giaccio et al., 2017)) and Y-6 ( $45.50 \pm 1$  ka (Zanchetta et al., 2018)) tephra units – each  
228 assumed to have been deposited instantaneously. The final model used herein presents the median  
229 of all the iterations (generally indistinguishable from the mean), and when referring to ages of specific  
230 depths within the core we include the 95% confidence intervals. The upper 2 m (Holocene) section of  
231 core Co1215 is chronologically well constrained by 10  $^{14}\text{C}$  dates and two tephra layers, with age  
232 uncertainties in this section ranging from ~5 to 580 years. Uncertainty increases with depth due to the  
233 lack of independent chronological anchors available. For example, three ESR dates for a shell  
234 fragment layer give an average age of  $73.6 \pm 7.7$  ka, and form the only tie point currently available  
235 below 8.5 m depth. All twenty-seven tie-points and accompanying chronological details are presented  
236 in **Text S13** and **Table S1**. Our revised model shows broad agreement with the interpolation-based  
237 chronology presented by Damaschke et al. (2013), and confirms that core Co1215 provides a  
238 continuous record of sedimentation over the past ~90-kyr (**Fig. S1**), with each 2 cm sample equating  
239 to ~100 years.

240

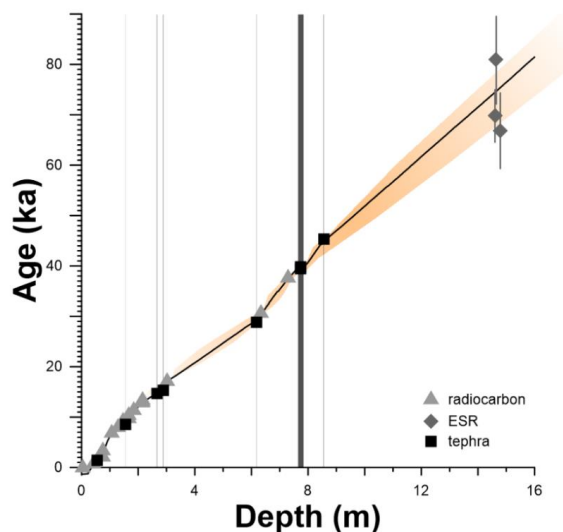


**Figure 3:** A Bayesian age-depth model for core Co1215 from Lake Prespa. Calibrated ages for the twenty-seven tie points used in model generation are displayed by type: radiocarbon-dated bulk organic, fish, or aquatic plant remains (light grey triangles), volcanic tephra layers (black squares) and electron-spin resonance (ESR)-derived dates for a shell layer (*Dreissena*) located at 14.63–14.58 m depth (dark grey diamonds). Uncertainties for ESR dates at  $1\sigma$  are presented as dark grey vertical lines. Black line marks the median core age predicted by the model, which is generally indistinguishable from the predicted mean. Minimum and maximum model ages at 95% ( $2\sigma$ ) confidence are marked with orange shading. Grey bars mark the stratigraphic placement of tephra layers used as tie-points, and widths of these bars are proportional to the thickness of the tephra layers within the core, respectively. Uncertainties for radiocarbon and tephra dates are within the displayed point sizes, and presented in **Table S2**.

241

242

### 243 3.2. Lake Ohrid (core 5045-1)

244 The 5045-1 coring site (“DEEP”) is located in the central part of Lake Ohrid (41°02’57” N, 20°42’54” E)  
 245 (Fig. 2). The uppermost 1.5 m of sediments at DEEP were recovered in 2011 using a UWITEC  
 246 gravity and piston corer. In 2013, sediments below 1.5 m depth were recovered from six closely-  
 247 spaced drill holes at the site (5045-1A to 5045-1F (Francke et al., 2016)). Sediment cores were  
 248 spliced to a composite record using optical and geochemical information. For sedimentological and  
 249 geochemical analyses, 2 cm thick slices (40.7 cm<sup>3</sup>) were removed from the core at a resolution of 16  
 250 cm (~480-yr) at the University of Cologne. For this study, we analysed 217 samples from between 0  
 251 and 36.27 m composite depth. We cannot entirely rule out that changes in sedimentation occurred  
 252 between samples, however, recent seismic (Lindhorst et al., 2015), borehole logging (Ulfers et al.,  
 253 2022) and sedimentological studies (Wagner et al., 2022, 2019) suggest that sedimentation at the  
 254 DEEP site has been near-continuous since ~1.3 Ma, with no clear evidence for any major (>1-kyr)  
 255 hiatuses. A detailed lithostratigraphic characterisation of the 5045-1 core succession is presented by  
 256 Francke et al. (2016). Details of the six microscopic and two visible tephra layers identified in the ~36  
 257 m section analysed in this study are presented by Leicher et al. (2021), and listed in **Table S3**.



258 The Lake Ohrid (5045-1) Hg data presented herein are paired with two previously existing datasets.  
259 The first dataset comprises TC and TIC measured using a DIMATOC 200, and TS using a Vario Micro  
260 Cube combustion CNS elemental analyser at the University of Cologne by Francke et al. (2016). TOC  
261 was calculated as the difference between TC and TIC (Francke et al., 2016; Wagner et al., 2019). The  
262 second dataset comprises XRF data using an ITRAX XRF core scanner at the University of Cologne  
263 at 2.56 m increments carried out on 2 cm thick samples, and processed using QSpec 6.5 software  
264 (Cox Analytical, Sweden). Elemental intensities were obtained for K, Ti, Fe, zirconium (Zr), and Ca  
265 (Francke et al., 2016; Wagner et al., 2019). To validate the quality of the XRF scanning data,  
266 conventional wavelength dispersive XRF (WDXRF, Philips PW 2400, Panalytical Cor., the  
267 Netherlands) was conducted on the 2-cm-thick samples at 2.56-m resolution. ITRAX data for each 2-  
268 cm-thick WDXRF sample was averaged to ensure comparability with the conventional XRF data, and  
269  $r^2$  values were to compare ITRAX and WDXRF datasets (full analytical details in Francke et al.  
270 (2016)).

271

### 272 3.2.1. Chronology

273 This study uses the age-depth model generated by Francke et al. (2016), and extended by Wagner et  
274 al. (2019) for the upper ~248 m and ~447 m of core 5045-1, respectively. Both combined  
275 tephrochronological data with orbital parameters using a Bayesian age modelling approach (Bacon  
276 2.269). Tephra layers were used as first-order constraints. From the eleven total  $^{39}\text{Ar}/^{40}\text{Ar}$  dated  
277 tephra layers employed in Wagner et al. (2019), seven are found in the upper ~36 m section analysed  
278 in this study (**Table S4**). The age of the eighth tie-point (OH-DP-0009) is defined following  
279 geochemical correlation of this tephra layer to the AD472/512 eruption of Somma-Vesuvius, Italy  
280 (Francke et al., 2019; Leicher et al., 2021). This chronological information was coupled with climate-  
281 sensitive proxy data (TOC and TIC) to define cross-correlation/inflection points with orbital  
282 parameters, which were included in the age–depth model as second-order constraints (**Table S4**).  
283 Four of these points correspond to the ~36 m interval analysed in this study (Wagner et al., 2019).  
284 The 95% confidence intervals of ages for specific depths produced by the model average at  $\pm 5.5$  kyr,  
285 with a maximum of  $\pm 10.6$  kyr. The resulting chronology suggests that the 0.97–36.27 m core section  
286 analysed here covers the time interval 1.6 – 89.6 ka, with each sample possessing a resolution of  
287 ~400 years (Francke et al., 2016; Wagner et al., 2019).

288

### 289 3.3. Mercury measurements

290 Total Hg concentrations ( $\text{Hg}_T$ ) in the bulk sediments of cores 5045-1 (Ohrid) and Co1215 (Prespa)  
291 were measured using a RA-915 Portable Mercury Analyzer with PYRO-915 Pyrolyzer, Lumex (Bin et  
292 al., 2001) at the University of Oxford. Samples were analysed for  $\text{Hg}_T$  at a resolution of ~2 cm for  
293 Lake Prespa, and ~16 cm for 5045-1 (see sections 3.1 and 3.2). Powdered samples were weighed  
294 into glass measuring boats, placed into the pyrolyzer (Mode 1) and heated to ~700°C, volatilizing any



295 Hg in the sample. Spectral analysis of the gases produced yields the total Hg content of the sample.  
296 Six measures of standard material (paint-contaminated soil – NIST Standard Reference Material ©  
297 2587) with a known Hg value of 290 ng g<sup>-1</sup> were run to calibrate the instrument prior to sample  
298 analysis, and then one standard for every 10 lacustrine samples (calibration results in  
299 **Supplementary Information**). Long-term observations of standard measurements with total Hg yield  
300 similar to the sediment samples analysed here indicate reproducibility is ±10% or better (Frieling et  
301 al., 2023).

302

### 303 **3.3.1. Mercury accumulation**

304 Rates of Hg accumulation in both cores were calculated by:

$$305 \quad Hg_{AR} = Hg_T (DBD * SR) \quad (eqn. 1)$$

306 where Hg<sub>AR</sub> is the total Hg mass accumulation rate (mg m<sup>-2</sup> kyr<sup>-1</sup>), Hg<sub>T</sub> is the total mercury  
307 concentration (expressed in mg g<sup>-1</sup>), DBD is the dry bulk density (g m<sup>-3</sup>), and SR is the sedimentation  
308 rate (m kyr<sup>-1</sup>). Values for Hg<sub>AR</sub> are also calculated with respect to the median age estimate for each  
309 sample, meaning that uncertainties increase with depth.

310 For Lake Prespa, we calculate the sedimentation rate using the updated age model presented in  
311 **section 3.1.2**. To calculate DBD, we employed the formula:

$$312 \quad DBD = M_{solid} / V_{total} \quad (eqn. 2)$$

313 where M<sub>solid</sub> is the mass of dry solid material (g) measured in each sample, and V<sub>total</sub> is the volume of  
314 each respective sample (2 cm<sup>3</sup>). Values for M<sub>solid</sub> were calculated based on recorded weight loss  
315 between wet and dry samples taken for CNS analyses by Aufgebauer et al. (2012).

316 For Lake Ohrid, we utilise the sedimentation rate values calculated by Wagner et al. (2019), and dry  
317 bulk density measurements measured by Francke et al. (2016) (see these publications for full  
318 methods).

319

### 320 **3.4. Mercury normalization**

321 The availability of specific host phases is often assumed to exert control on the sedimentary burial of  
322 Hg. Here, we test if the Hg deposited into the sediments of lakes Prespa and Ohrid may be impacted  
323 by abundance of a suite of phases. To do this, we assess both Hg<sub>T</sub> records relative to quantitative  
324 estimates of TOC and TS (assuming sulphides contribute to TS): both considered potential host  
325 phases of Hg in sedimentary successions (Chakraborty et al., 2015; Garcia-Ordiales et al., 2018;  
326 Ravichandran, 2004; Shen et al., 2020).

327 Detrital minerals constitute another potential host phase of Hg in sedimentary records. Elements such  
328 as Al, Ti, K, Zr, and Rb are commonly used as proxies for this purpose (Kongchum et al., 2011;



329 Percival et al., 2018b; Shen et al., 2020). We observe a close correlation between K and Ti in Lake  
330 Prespa, and quartz in Lake Ohrid (**Fig. S2**): all proxies for fine-grained material inputs to a lake basin  
331 (Grygar et al., 2019; Warrior et al., 2016). To facilitate direct comparison of the two cores, we assess  
332 the relative abundances of (fine-grained) detrital material using XRF-based K counts. To account for  
333 differences in resolution between Hg and XRF data, K measurements were averaged to the thickness  
334 of each discrete Hg sample, and K values corresponding to the Hg sample depths extracted.

335 In line with previous studies (Shen et al., 2020), we assume that the strongest positive-sloped linear  
336 correlation with Hg among the analysed elements TS, TOC, and K signals the most likely dominant  
337 influence on Hg loading in each core, which may then be interpreted as the 'host-phase'. However, it  
338 is conceivable that different host phases may dominate in different sections of the individual cores or  
339 that no single host-phase clearly dominates, and so the same approach is also applied restricted to  
340 the data within each individual marine isotope stage (MIS) (**Table 1**).

341

## 342 **4. Results & Discussion**

343 Sediment cores extracted from Lake Prespa (Co1215) and Lake Ohrid (5045-1) provide a detailed,  
344 time-resolved record of Hg cycling between -90 and 0 ka. Results are presented with direct reference  
345 to key stratigraphic intervals: the Holocene (12–0 ka; MIS 1), and the late Pleistocene (120 –12 ka;  
346 MIS 2–5). Evidence for interglacial climatic conditions marks the start of the Holocene epoch (~12 ka)  
347 in SE Europe (Kern et al., 2022; Panagiotopoulos et al., 2014; Sadori et al., 2016; Tzedakis et al.,  
348 2006). For simplicity, we hereafter equate "MIS 1" to the Holocene, allowing a clearer distinction  
349 between glacial (late Pleistocene) and interglacial (Holocene) climate conditions. We use these time-  
350 slices, that also represent broad climate and environmental 'modes', as a framework upon which the  
351 Hg composition of both cores can be directly compared relative to local changes in sediment lithology  
352 and geochemistry (**Table 1**), and a foundation upon which local and regional-scale environmental  
353 changes can be assessed relative to global shifts in glaciation, climate, sea level, and ocean  
354 circulation.

355



356 **Table 1:** A comparison of cores Co1215 (Lake Prespa) and 5045-1 (Lake Ohrid) relative to the late Pleistocene (LP; 120 – 12  
 357 ka), the Holocene (H; 12 – 0 ka), and the marine isotope stage (MIS) stratigraphic framework defined in Lisiecki & Raymo  
 358 (2005)\*. Hg<sub>T</sub> is given in ng g<sup>-1</sup>, and Hg<sub>AR</sub> is given in mg m<sup>-2</sup> kyr<sup>-1</sup>.

			Depth (m)	Mean		Sedimentology**	
				Hg <sub>T</sub>	Hg <sub>AR</sub>	Lithology	Key Features
Lake Prespa	Holocene	MIS 1	2.4–0	64.6	34.7	Silt gyttja. Decreasing sand content with depth.	High lake levels. One visible and one microscopic tephra layer. High microcharcoal and green algae concentrations. High TOC/TN ratios. High sedimentation rate.
	Late Pleistocene	MIS 2	6–2.4	41.9	16.4	<b>2.9–2.4 m</b> – High fine sand (<250 µm), with clayey silt and evidence of lamination. <b>6–2.9 m</b> – Homogenous sediment structure. Silt, distinct lamination and siderite precipitation.	Increasing lake level. Two cryptotephra layers. Transient nutrient pulse 12.8–11.7 ka. Moderate TOC and low TIC. Evidence for ice-rafted debris deposition. Low productivity and lake level. High K and organic δ <sup>13</sup> C. Low water δ <sup>18</sup> O. Declining C/N ratios. High sedimentation rate.
		MIS 3	11–6.1	32.8	8.9	<b>6.6–6.1 m</b> - Massive sediment structure. Silt with distinct lamination. <b>11–6.6 m</b> – Massive sediment structure. Silt.	Steady decrease in lake level. High oxygen index. Increasing lake level. Four visible and three microscopic tephra layers. High C/N ratios. Moderate TOC, very low TIC.
		MIS 4	13.9–11	33.7	10.4	Massive sediment structure. Clayey silt.	High sedimentation rate. Very low TOC. No tephra layers. Low productivity. Declining C/N ratios. High K content gives evidence for ice-rafted debris deposition.
		MIS 5a-c	17.7–13.9	44.2	13.3	<b>15.2–13.9 m</b> - Massive, bioturbated sediments. Clayey silt and fine sand. <b>17.8–15.2 m</b> – Massive sediment structure. Clayey silt with fine sand (a).	Increasing lake level and high productivity. <i>Dreissena</i> shell layer 14.58–14.56 m. Deep lake with moderate/low productivity High green algae concentrations. High TOC, low TIC.
Lake Ohrid	Holocene	MIS 1	4.6 – 1.1	47.2	26.2	<b>3–0 m</b> – Massive sediment structure. Bright colouring indicates high calcite; dark colouring indicates lower calcite.	High productivity. Four microscopic tephra layers. Low K concentrations. High sedimentation rate.
						<b>4.6–3 m</b> – Slightly calcareous silty clay and massive sediment structure. Frequent siderite-rich layers.	Low TIC and calcite. High iron availability. Low productivity and stronger calcite dissolution. High K concentrations. High sedimentation rate.
	Late Pleistocene	MIS 2	11.3 – 4.6	69.2	45.5	Silty clay. Mottled, often massive sediment structure. Frequent siderite-rich layers. Abundant fine fraction (< 4 µm) sediments.	Very low TIC, TOC, and calcite suggesting low productivity, with large inputs of fine-grained, and chemically weathered siliciclastics. High iron availability. Two visible and two microscopic tephra layers. Mass-movement deposit at 7.87 m.
		MIS 3	23–11.3	50.6	33.4		
		MIS 4	28.8–23	50.2	29.6		
		MIS 5a-c	36.3–28.8	36	20.4	<b>35.6 – 28.8 m</b> – Silty clay with a massive sediment structure. Bright colouring indicates high calcite; dark colouring indicates lower calcite. <b>36.6 – 35.6 m</b> – Silty clay. Mottled, often massive sediment structure. Frequent siderite-rich layers.	Low siliciclastic mineral abundance. Decreasing δ <sup>18</sup> O and δ <sup>13</sup> C. Strong primary productivity. Low sedimentation rate. Higher carbonate δ <sup>18</sup> O and δ <sup>13</sup> C corresponds to reduced TIC, and high siderite. Low sedimentation rate.

359

360 \* MIS 5a-c – 96–71 ka; MIS 4 – 71–57 ka; MIS 3 – 57–29 ka; MIS 2 – 29–12 ka; MIS 1 – 12–0 ka.

361 \*\*Summarised from the following references:



362 **Lake Prespa** - (Aufgebauer et al., 2012; Cvetkoska et al., 2015; Damaschke et al., 2013; Leng et al., 2013; Panagiotopoulos et al., 2014; Wagner  
 363 et al., 2014)  
 364 **Lake Ohrid** - (Francke et al., 2016, 2019; Just et al., 2015; Lacey et al., 2016; Leicher et al., 2021; Wagner et al., 2019)  
 365

#### 366 4.1. Host Phase Controls

367 The availability and abundance of specific host phases is often assumed to control sedimentary Hg  
 368 accumulation and burial (Shen et al., 2020). Both Lake Prespa and Lake Ohrid show evidence for  
 369 complex relationships between  $Hg_T$ , TOC, TS, and K concentrations through time (**Fig. 4**). However,  
 370 the trends displayed in **Figure 4** also suggest that: (1) the strength of the relationships between Hg,  
 371 TOC, TS, and detrital minerals (K) are distinctly different between the two lakes, and (2) the  $Hg_T$   
 372 signals preserved in Lake Prespa and Lake Ohrid cannot be fully explained by variability in  
 373 abundance of these potential host phases individually.

374

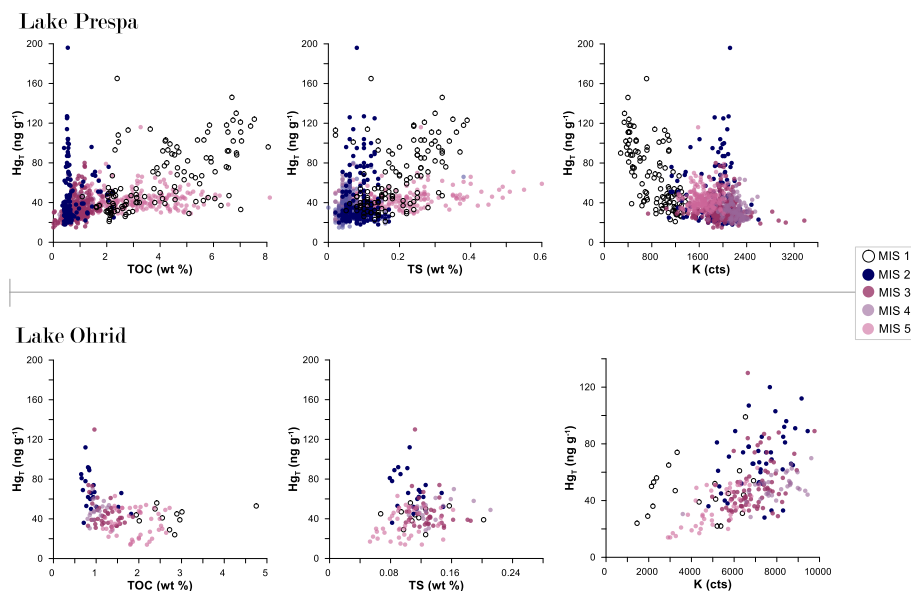


**Figure 4:** A comparison of host-phase relationships between lakes Prespa and Ohrid. Points are colour-coded relative to stratigraphic period: the Holocene (12–0 ka, transparent circles), and the late Pleistocene (90–12 ka, filled circles). We compare  $Hg_T$  records for both lakes relative to total organic carbon (TOC), sulphide (estimated by total sulphur (TS)), and detrital minerals (estimated by potassium (K) concentrations) – note that aluminium (Al) data are more commonly used as an indicator of detrital mineral abundance but these are currently unavailable for 5045-1.

375

376 Core Co1215 from Lake Prespa shows a moderate correlation between  $Hg_T$  and TOC during the  
 377 Holocene and late Pleistocene (all data in **Fig. 4**; **Table 1**). This correlation is most significant during  
 378 the Holocene (MIS 1), where distinct enrichments in  $Hg_T$  occur in conjunction with a similarly sharp  
 379 increase in TOC, and low variability in Hg/TOC values (**Fig. 5**). However, it is more inconsistent during



380 the late Pleistocene (MIS 2–5). For example, the highest  $Hg_T$  values are measured in the relatively  
381 TOC-lean sediments of MIS 2 (**Fig. 4, 5**), and a plateau also appears when higher TOC  
382 concentrations are reached during MIS 5 whereby  $Hg_T$  no longer increased in step with TOC (**Fig. 4,**  
383 **S2**). The correlations observed are not strong enough to conclude that TOC availability can fully  
384 explain the Hg signals observed in Lake Prespa throughout the 90-kyr succession.

385 Correlations between  $Hg_T$ , detrital mineral and/or TS availability are also largely absent, suggesting  
386 that the complex Hg/TOC relationship is not a function of time-varying sulphides and detrital mineral  
387 availability. Large peaks in Hg/K are visible during the Holocene (**Fig. 5**), but these are not reflected in  
388  $Hg_{AR}$  and therefore an artefact of considerably lower K concentrations within this section of the core  
389 rather than indicators of changes in lake Hg levels. The highest positive  $r^2$  value between  $Hg_T$  and TS  
390 is observed during the Holocene (MIS 1:  $r^2 = 0.25$ ) (**Fig. 4**), implying that >75 % of variance in the  
391 dataset cannot be explained with sulphide availability during this time period. Correlations for other  
392 periods are even weaker and some periods appear to show distinct patterns of Hg and potential host-  
393 phase behaviour (**Fig. 4**). This could imply that our Hg data captures: (1) catchment-driven shifts in  
394 sources of organic matter and detrital material deposited into the lake (Leng et al., 2013), and/or (2)  
395 significant changes in the overall availability of Hg in the environment through time (e.g., due to a  
396 change in rates of Hg emission and/or exchange between (local) surface reservoirs (Bishop et al.,  
397 2020)). Nonetheless, Hg variability in the Prespa Hg dataset cannot be fully explained by changes in  
398 organic matter, sulphur, or detrital mineral content (**Fig. 4**), implying that Hg flux, rather than host  
399 phase availability, controls Hg sequestration in Lake Prespa.

400

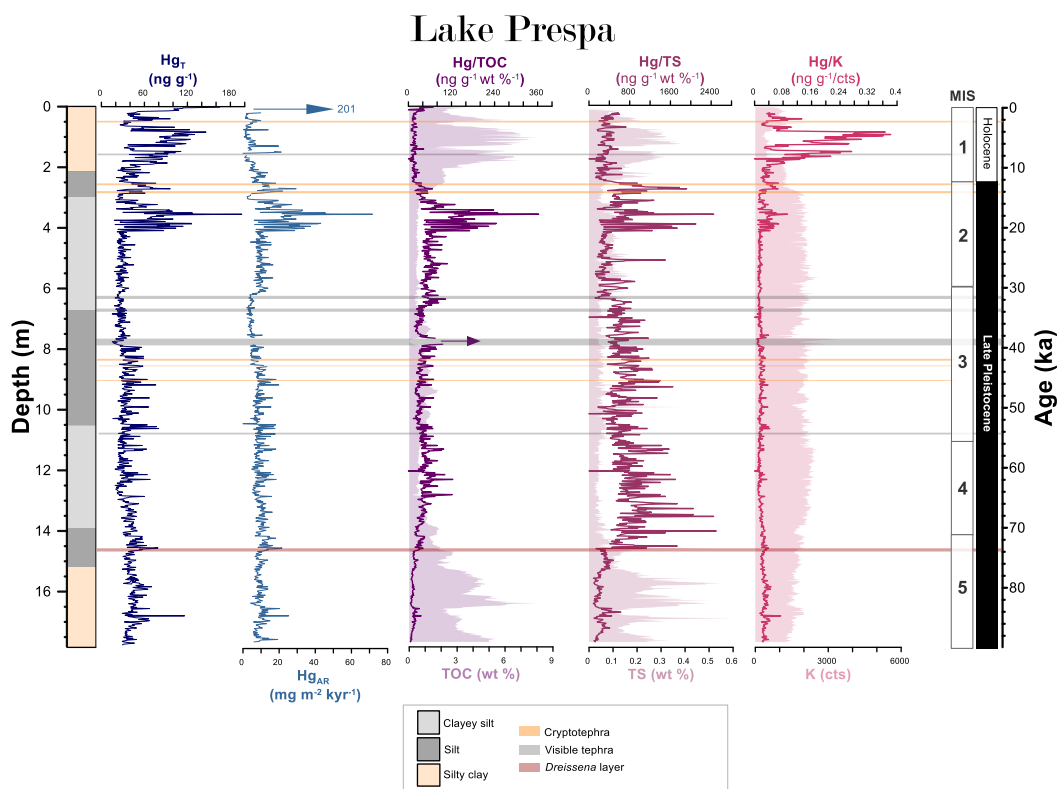


**Figure 5:** Total Hg ( $Hg_T$ ) and total Hg accumulation rate ( $Hg_{AR}$ ) for core Co1215 from Lake Prespa, presented as a function of depth and time, and relative to lithofacies, visible (grey shading) and cryptotephra (orange shading) layers. We include records of  $Hg_T$  (this study) normalized to records of total organic carbon (TOC) (Damaschke et al., 2013), sulphide (estimated by total sulphur (TS)) (Aufgebauer et al., 2012), and detrital mineral abundance (estimated by potassium (K)) (Panagiotopoulos et al., 2014), with filled shading marking the original datasets. A distinct lake low stand based on seismic profiles and sedimentological data is marked at 14.63 - 14.58 m depth (red shading) (Wagner et al., 2014). A purple arrow marks sections where artificially high  $Hg/TOC$  values are generated by a sharp drop to near-zero TOC (<0.06 wt %) coinciding with deposition of the Y-5 (17.1 m) tephra unit – an effect expected as background sedimentation is interrupted by volcanic ash deposition. White boxes mark the marine isotope stages defined by (Lisiecki and Raymo, 2005), and stratigraphic periods are labelled in black/white.

401

402 Core 5045-1 from Lake Ohrid shows elevated  $Hg_T$  during the late Pleistocene compared to the  
 403 Holocene (**Fig. 6; Table 1**). Peaks in  $Hg_T$  most consistently correspond to increases in K (detrital  
 404 mineral) intensities, reflected in a broadly positive relationship between  $Hg_T$  and K throughout the  
 405 succession (**Fig. 4, S3**). However, this relationship is only described by  $r^2$  values <0.5 and the  
 406 strength of this correlation varies across the span of the record, weakening during the Holocene (**Fig.**  
 407 **4**).

408 Variable Hg values in the Ohrid record appear less influenced by organic matter and/or sulphide  
 409 availability. Fluctuations in TOC/TS values suggest that some sulphide formation may have occurred  
 410 during the late Pleistocene (MIS 2-5) (Wagner et al., 2009; Francke et al., 2016). However, even in  
 411 these phases, TS remains low and correlations between  $Hg_T$  and TS are generally negative or weak  
 412 ( $r^2 < 0.2$ ; **Fig. 4**) so that Hg signals do not change in magnitude or expression even when TS



413 variability is accounted for (Fig. 6), potentially due to the oligotrophic state of Lake Ohrid favouring  
 414 burial of sulphide-depleted sediments (Francke et al., 2016; Vogel et al., 2010). More remarkable, the  
 415 relationship between  $Hg_T$  and organic matter in Lake Ohrid also shows an inverse correlation (Fig. 4)  
 416 somewhat reminiscent of a trend observed in the uppermost sediments of a ~5 Ma succession from  
 417 Lake Baikal (Russia) (Gelety et al., 2007). These trends may be explained by a scenario where the  
 418 Hg flux to Ohrid from direct deposition and/or surrounding catchment is typically the limiting factor,  
 419 rather than availability of potential host phases.

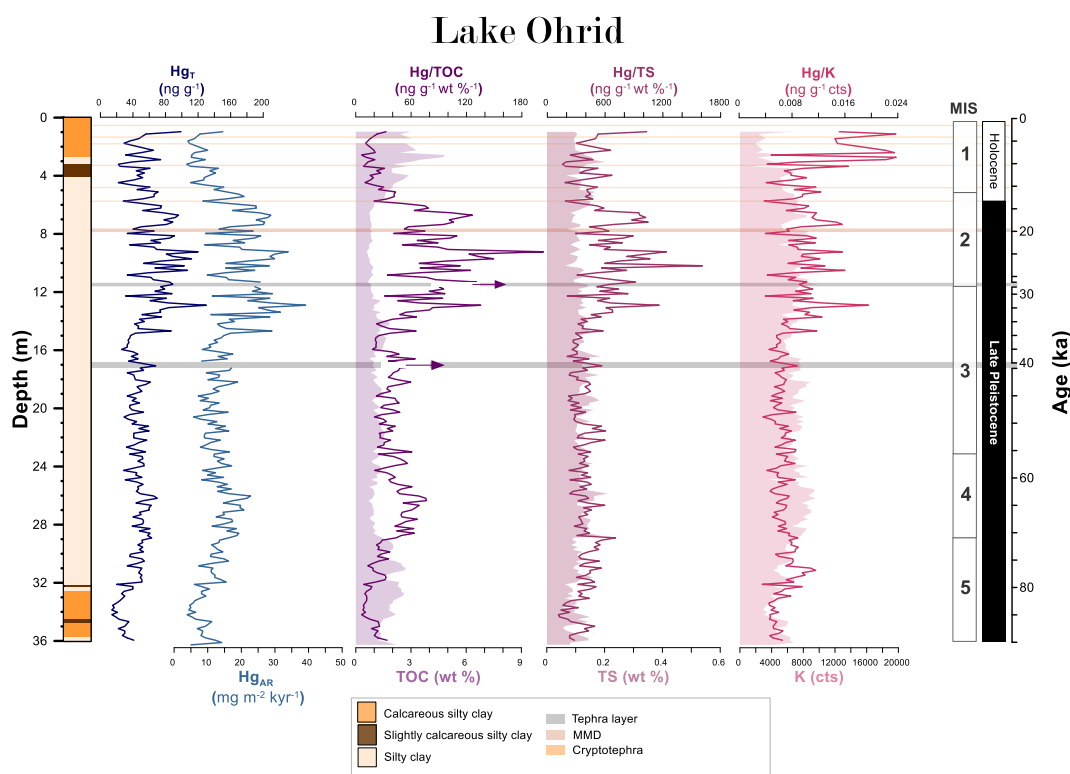


**Figure 6:** Total Hg ( $Hg_T$ ) and total Hg accumulation rate ( $Hg_{AR}$ ) for core 5045-1 from Lake Ohrid, presented as a function of depth and time, and relative to lithofacies, visible (grey shading) and cryptotephra (orange shading) layers. We include records of  $Hg_T$  (this study) normalized to records of total organic carbon (TOC) (Francke et al., 2016), sulphide (estimated by total sulphur (TS)) (Francke et al., 2016), and detrital mineral abundance (estimated by potassium (K)) (Francke et al., 2016; Wagner et al., 2019), with filled shading marking the original datasets. A mass movement deposit (MMD) is marked at 7.87 m depth (brown shading) (Francke et al., 2016). Purple arrows mark sections where artificially high  $Hg/TOC$  values are generated by a sharp drop to near-zero TOC (<0.06 wt %) coinciding with deposition of the Y-5 (17.1 m) and Mercato (11.5 m) tephra layers – an effect expected as background sedimentation is interrupted by volcanic ash deposition. White boxes mark the marine isotope stages as defined by Lisiecki and Raymo (2005), and stratigraphic periods are labelled in black/white.

420

421 Lake Ohrid and Lake Prespa show distinct differences in the strength of their Hg-host phase  
 422 relationships. In Lake Prespa, Hg broadly covaries with organic matter (TOC), whereas in Lake Ohrid  
 423 correlations are observed between Hg and detrital minerals (K). Nonetheless, only a relatively small  
 424 proportion of Hg variability can be explained by host phase availability in each record. This suggests  
 425 that while host phase availability may, at times, exert influence on the Hg signals recorded in these



426 lakes, the catchment-controlled changes in Hg fluxes are typically the more dominant effect on Hg in  
427 these sediment records. We therefore surmise that the  $Hg_T$  and  $Hg_{AR}$  signals recorded in Lake Prespa  
428 and Lake Ohrid are records of net Hg input to the two lakes rather than the efficiency of sedimentary  
429 drawdown.

430

#### 431 **4.2. Tephra layers**

432 As volcanic eruptions are among the most significant natural Hg sources we assess whether the  
433 previously recognized tephra deposition events in Lake Prespa correspond to changes in Hg  
434 deposition. Overall, we find that individual tephra horizons and surrounding sediments do not  
435 consistently correspond to measurable peaks in  $Hg_T$  or  $Hg_{AR}$  in Lake Prespa (**Fig. 5**). Despite a  
436 resolution of <100-years per sample, only two of the eleven preserved ash layers coincide with  
437 elevated  $Hg_T$ : Mercato ( $8.54 \pm 0.09$  ka; Somma-Vesuvius), and LN1 ( $14.75 \pm 0.52$  ka; Campi Flegrei).  
438 These two units are not associated with disproportionately large tephra volumes and neither coincide  
439 with evidence for transient changes in authigenic carbonate precipitation or sediment diagenesis that  
440 may impact sedimentary Hg. This implies that Hg concentrations in Lake Prespa cannot, in general,  
441 be unequivocally linked to short-lived (<1-year) individual eruption events between ~90 and 0 ka (**Fig.**  
442 **S5**).

443 Discrete ash fall events (recorded by tephra/cryptotephra) do not consistently correspond to  
444 measurable peaks in  $Hg_T$  or  $Hg_{AR}$  in the slightly lower-resolution (~400-yr per sample) Lake Ohrid  
445 record (**Fig. S5**). Considering this lack of correspondence of Hg with ash layers, in conjunction with  
446 the Lake Prespa data too, suggests that (a) surface Hg loading was not appreciably increased with  
447 most large eruption events over the past 90 kyr in the Balkans and/or (b) sampling resolution may  
448 need to be significantly higher and/or focused on lesser-bioturbated records to identify single, short-  
449 lived volcanogenic perturbations of the scale and type occurring during the period recorded in the  
450 Ohrid (and Prespa) sedimentary successions.

451



452 4.3. Variability through time

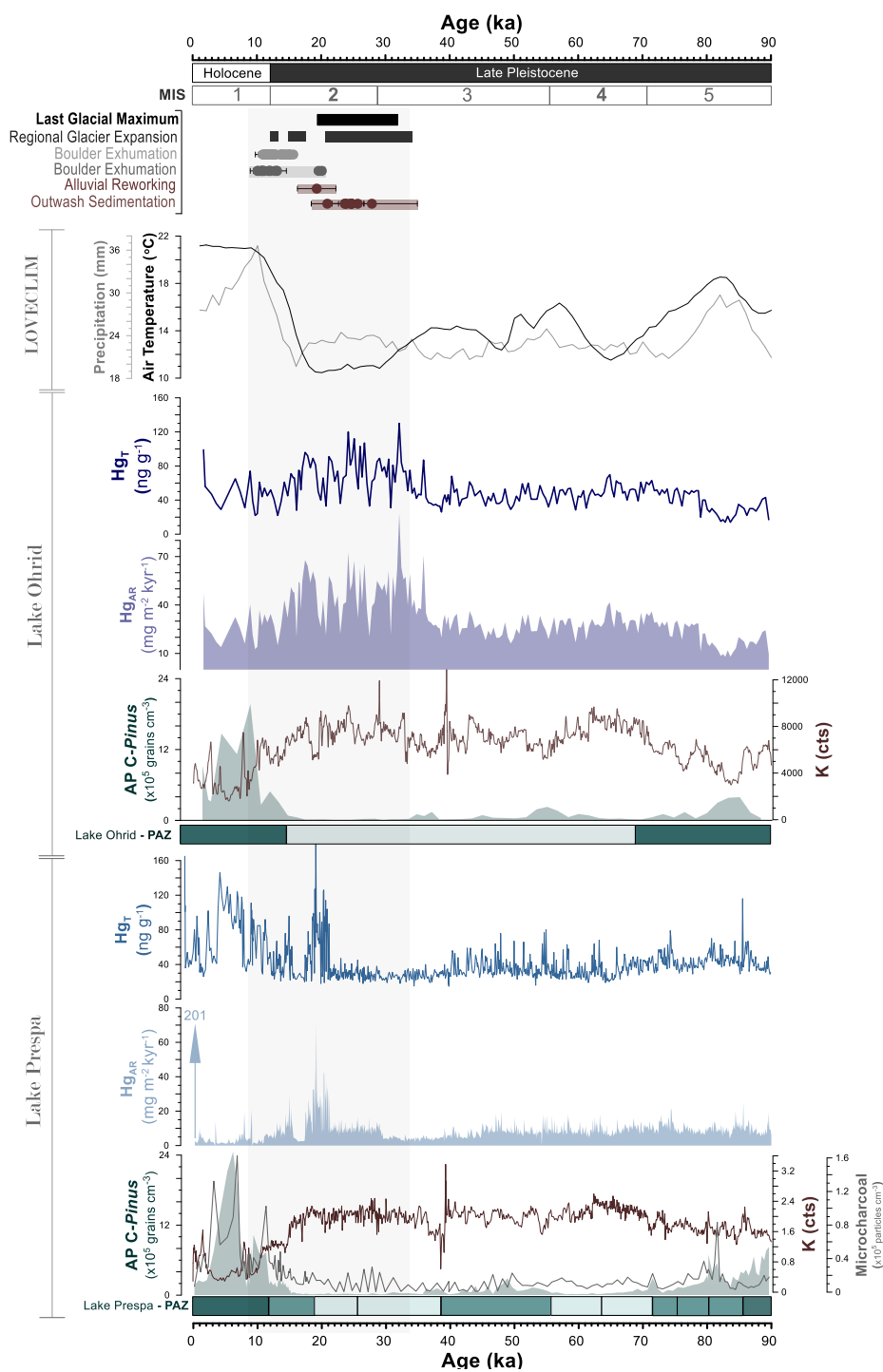




**Figure 7:** Total mercury ( $Hg_T$ ) and mercury accumulation rate ( $Hg_{AR}$ ) records for Lake Prespa and Lake Ohrid generated by this study and proxy datasets generated by prior studies. For Lake Prespa, these include arboreal pollen (AP) concentrations (Panagiotopoulos et al., 2014), microcharcoal (Panagiotopoulos, 2013), potassium (K) (Aufgebauer et al., 2012; Wagner et al., 2010), and pollen assemblage zones (PAZ) (Panagiotopoulos et al., 2014). For Lake Ohrid, these include AP concentrations (Sadori et al., 2016), potassium (K) (Wagner et al., 2019; Francke et al., 2016), 1000-year average surface-air temperature (SAT - °C) and annual mean precipitation (millimetres) both simulated by the LOVECLIM Earth system model (Goosse et al., 2010) for the Prespa/Ohrid region (Wagner et al., 2019), and pollen assemblage zones (PAZ) (Sadori et al., 2016). Pollen assemblage zones defined by Panagiotopoulos et al. (2014) (Lake Prespa) and Sadori et al. (2016) (Lake Ohrid) are presented as green bars, shaded relative to tree population density (darker colour = higher density). We include a chronology of glacial processes based on radiometric dating of glacial landforms in the following locations: the Voidomaitis river basin (purple) (Lewin et al., 1991; Woodward et al., 2008), the Pindus Mountains (lilac) (Allard et al., 2021, 2020; Styllas et al., 2018; Hughes et al., 2006; Pope et al., 2017), and the Dinaric Alps (blue) (Gromig et al., 2018; Ribolini et al., 2018; Ruzkiczay-Rüdiger et al., 2020). White boxes mark the marine isotope stages (MIS) as defined by Lisiecki and Raymo (2005), and stratigraphic periods are labelled in black/white. Vertical grey shading denotes the timing of the largest changes in glacier extent and volume.

453

#### 454 **4.3.1. Late Pleistocene (90 – 35 ka; MIS 5 to MIS3)**

455 The Lake Prespa and Lake Ohrid sediment cores show similarly muted variability in  $Hg_T$  and  $Hg_{AR}$   
456 values between ~90 and 35 ka (broadly MIS 5a-c, 4 & 3), alluding to relatively stable Hg inputs (**Fig.**  
457 **7; Table 1**). High organic and low clastic material concentrations point to warmer climate conditions  
458 during this interval, in which both catchments experienced an increase in moisture availability,  
459 pronounced forest expansion, and plant diversification – collectively acting to stabilize hillslopes and  
460 reduce deep soil erosion (Francke et al., 2019; Panagiotopoulos et al., 2014; Sadori et al., 2016,  
461 2016). One possibility is that Hg sequestration during this interval was controlled by consistent rates  
462 of algal scavenging (Biester et al., 2018; Outridge et al., 2007, 2019; Stern et al., 2009). Elevated  
463 TOC (**Fig. 5**), hydrogen index, TOC/TN, and biogenic carbonate concentrations between ~90 and 71  
464 ka in both Lake Prespa and Lake Ohrid signal nutrient upwelling and increased allochthonous inputs,  
465 in conjunction with elevated primary productivity. For example, Lake Prespa records green algae  
466 accumulation (Cvetkoska et al., 2016, 2015; Leng et al., 2013; Panagiotopoulos et al., 2014), and  
467 sediments rich in biogenic silica ( $bSiO_2$ ) are also visible in Lake Ohrid (Francke et al., 2016). Slow  
468 changes in lake geochemistry associated with these biological processes are consistent with a steady  
469  $Hg_{AR}$  in both Lake Prespa and Lake Ohrid during this time, and absence of any especially pronounced  
470 changes in  $Hg_T$ . This could suggest that, for a relatively prolonged period (~96–35 ka), Hg flux to the  
471 two lakes did not change with a magnitude sufficient to cause measurable sedimentary changes, and  
472 processes capable of amplifying differences in sedimentary Hg between Ohrid and Prespa were not  
473 particularly influential.

474 MIS 3 marks the start of slow divergence between the Hg records of Lake Prespa and Lake Ohrid.  
475 Although often referred to as an 'interglacial', MIS 3 exhibits a distinctly more 'glacial' climate  
476 signature that is more comparable to MIS 4 in the Prespa/Ohrid region, for which proxy records point  
477 to a regional climate regime that was characterized by distinctly cooler, and also drier climatic  
478 conditions (**Fig. 7**) (Panagiotopoulos et al., 2014; Sadori et al., 2016; Wagner et al., 2019). Divergent  
479 Hg signals could be linked to two climate-driven processes. First, a reduction in primary productivity in



480 Lake Prespa signalled by decreasing TOC, hydrogen index, and endogenic carbonate compared to  
481 values observed during MIS 5 (Aufgebauer et al., 2012; Cvetkoska et al., 2016; Leng et al., 2013).  
482 Second is an increase in detrital material flux to both lakes (signalled by elevated K count; **Fig. 7**),  
483 due to recession of the surrounding forests and subsequently elevated rates of catchment erosion  
484 (Damaschke et al., 2013; Francke et al., 2019; Panagiotopoulos et al., 2014; Sadori et al., 2016). This  
485 environmental shift is more likely to favour enhanced Hg mobility in the catchment and burial in a  
486 system whereby detrital minerals could either constitute the primary host phase or correlate to Hg<sub>T</sub>;  
487 and so could explain the progressive elevation in Hg<sub>T</sub> and Hg<sub>AR</sub> observed in Lake Ohrid (**Fig. 4**).

488

#### 489 **4.3.2. Last Glaciation (35–12 ka; MIS 3 to MIS2)**

490 The timing, amplitude, and expression of Hg signals captured in Lake Prespa and Lake Ohrid change  
491 significantly between ~35 and 12 ka (**Fig. 7**). The largest Hg<sub>T</sub> and Hg<sub>AR</sub> peaks in Lake Ohrid coincide  
492 with the Last Glacial Maximum (LGM), and begin at ~35 ka (**Fig. 7**). Synchronous enrichments in K,  
493 quartz, and Ti (Francke et al., 2016; Wagner et al., 2019) provide evidence for elevated clastic  
494 terrigenous matter inputs and erosion, and are consistent with evidence for a significantly less-  
495 vegetated catchment (Donders et al., 2021; Sadori et al., 2016). High clastic fluxes into the lake  
496 during the LGM could also relate to meltwater run-off from local mountain glaciers (Ribolini et al.,  
497 2011), which would transport large volumes of sediment generated by glacial abrasion, quarrying and  
498 plucking (Carrivick and Tweed, 2021; Overeem et al., 2017) into the lake basin. Given that Hg  
499 sequestration in Lake Ohrid appears partially related to the abundance of detrital minerals for much of  
500 the record (**Fig. 4, 5**), these Hg peaks could relate to local, climate-driven shifts in landscape structure  
501 associated with glaciation during MIS 2 (**Fig. 4, 7**).

502 Alternatively or in addition to these local effects, atmospheric mineral dust concentrations were also  
503 up to twenty-times higher during the LGM (Simonsen et al., 2019). Mineral dust may be the most  
504 important Hg carrier in ice-cores (Jitaru et al., 2009; Vandal et al., 1993), and studies have shown  
505 evidence for notable redistribution of terrestrial Hg during the LGM owing to changes in regional  
506 atmospheric dust deposition (de Lacerda et al., 2017; Fadina et al., 2019; Pérez-Rodríguez et al.,  
507 2015). However, marine sediment records fail to capture measurable changes in dust fluxes over the  
508 Ionian and Aegean seas corresponding to MIS 2 (Ehrmann and Schmiedl, 2021). We also see no  
509 clear evidence atmospheric dust played a major (direct) role in the local Hg cycle in our data. For  
510 example, peaks in elemental ratios typically associated with mineral dust deposits (e.g., Zr/Ti) do not  
511 correspond to peaks in Hg<sub>T</sub> and/or Hg<sub>AR</sub> (Vogel et al., 2010), and marine sediment records also fail to  
512 capture measurable changes in dust fluxes over the Ionian and Aegean seas corresponding to  
513 pronounced Hg signals in Lake Ohrid (Ehrmann and Schmiedl, 2021). Therefore, we cannot  
514 mechanistically link elevated Hg values during MIS 2 in Lake Ohrid to broad-scale changes in  
515 atmospheric dust deposition.

516 The largest Hg<sub>T</sub> and Hg<sub>AR</sub> peaks in Lake Prespa occur between 21.3 ( $\pm 1.7$  ( $1\sigma$  from the Bayesian age  
517 model, see **Fig. 3**)) ka and 17.5 ( $\pm 0.7$ , ( $1\sigma$ )) ka. These signals do not correspond to a measurable



518 change in host phase availability (**Fig. 5**), so it is unlikely that these peaks reflect changes in TOC,  
519 TS, and/or K. However, they do coincide with deglaciation of the Pindus and Dinaric mountains (**Fig.**  
520 **7**) (Hughes et al., 2023). Geomorphological evidence suggests that glaciers were present across the  
521 Prespa/Ohrid region between ~26.5 and 15 ka (Belmecheri et al., 2009; Gromig et al., 2018; Ribolini  
522 et al., 2018; Ruzsiczay-Rüdiger et al., 2020), and indeed that periglacial processes created a  
523 landscape characterized by intense weathering, erosion and sediment transport (Hughes and  
524 Woodward, 2017; Allard et al., 2021). Glacial meltwaters thus likely constituted a major source of  
525 water input to Lake Prespa during the last deglaciation. Glaciers are important sinks for atmospheric  
526 Hg deposited by both dry and wet processes (Durnford and Dastoor, 2011; Zhang et al., 2012), and  
527 large quantities of Hg can accumulate in organic-rich frozen soils (permafrost, Schuster et al., 2018).  
528 High proportions of detrital matter within glacial ice, snow, and organic matter facilitate the effective,  
529 long-term (>100s-1000s of years) retention of atmospheric Hg, meaning that rapid snow/ice melt and  
530 permafrost thawing can produce transient 'pulses' of Hg into lakes without a comparable peak in  
531 sediment influx (Durnford and Dastoor, 2011; Kohler et al., 2022). This is consistent with the abrupt  
532 and short-lived expression of the Hg signal retained in Lake Prespa between 21.3 and 17.5 ( $\pm 1.7$ – $0.7$   
533 ( $1\sigma$ ) ka, which occurs in the absence of a pronounced change in terrigenous elements (e.g., Ti, Rb)  
534 or sulphides (**Fig. 5, 7**).

535 Although in Lake Ohrid  $Hg_{AR}$  is generally elevated during the LGM and deglaciation, a distinct Hg  
536 signal corresponding to deglaciation as recorded in Prespa is not captured (**Fig. 7**). Given their close  
537 proximity and environmental similarity, both lakes could be expected to record similar overall signals if  
538 the climate-driven processes influencing  $Hg_{AR}$  were broadly similar. Part of the disparity may relate to  
539 a change in the lake's hydrological connection to Lake Prespa (Cvetkoska et al., 2016; Jovanovska et  
540 al., 2016; Leng et al., 2010). Tracer experiments and stable isotope ( $\delta^{18}O$ ) analysis suggest that water  
541 draining from Lake Prespa accounts for a significant proportion of Lake Ohrid's water inflow alongside  
542 precipitation (Matzinger et al., 2006; Wagner et al., 2010; Lacey and Jones, 2018), with high rates of  
543 prior calcite precipitation occurring in the connecting karst system (Eftimi et al., 1999; Leng et al.,  
544 2010; Matzinger et al., 2006). However, decreases in the reconstructed  $\delta^{18}O$  of lakewater and TIC in  
545 both lakes during the last glaciation point to a reduction in the contribution of karst-fed waters to Lake  
546 Ohrid (Lacey et al., 2016; Leng et al., 2013). Although it is unlikely that the two hydrological systems  
547 became completely decoupled (Belmecheri et al., 2009; Lézine et al., 2010), evidence for permafrost  
548 formation at high elevations between 35 and 18 ka (Oliva et al., 2018; Van Vliet-Lanoë and  
549 Hallegouët, 2001) and lower precipitation (**Fig. 7**) could be linked to a reduction in karst aquifer  
550 activity. For Lake Prespa, a measurable change in lake volume would reduce the number (and  
551 pressure) of active sinkholes (Wagner et al., 2014), and subsequently the outflow of water and solutes  
552 (e.g., Hg) into Lake Ohrid. We speculate that this may result in higher rates of Hg accumulation in  
553 Lake Prespa during intervals of low lake level, where water inputs originated mainly from glacial  
554 meltwaters.

555 Neither Lake Ohrid nor Lake Prespa shows large Hg signals during the Oldest (17.5-14.5 ka) and  
556 Younger (12.9-11.7 ka) Dryas, despite evidence for an abrupt return of glacial conditions (Aufgebauer



557 et al., 2012; Cvetkoska et al., 2015; Panagiotopoulos et al., 2014) and local glacier stabilization  
558 (Gromig et al., 2018; Ribolini et al., 2018; Ruszkiczay-Rüdiger et al., 2020) (**Fig. 7**). We posit that  
559 these events were either too (a) short-lived, and/or (b) climatically mild to produce the same response  
560 in the terrestrial Hg cycle as the processes operating during, and immediately following, the LGM,  
561 which could explain the lack of an associated sedimentary signal.

562

### 563 **4.3.3. Holocene (12–0 ka; MIS1)**

564 The timing and amplitude of Hg<sub>T</sub> and Hg<sub>AR</sub> signals recorded in Lake Prespa and Lake Ohrid  
565 sediments are noticeably different during the Holocene interglacial (MIS 1). Between ~12 and 3 ( $\pm 0.5$ –  
566 0.2 ( $1\sigma$ )) ka, Lake Prespa captures a series of large peaks in Hg<sub>T</sub> and Hg<sub>AR</sub>, whereas these same  
567 proxies show a progressive decline in Lake Ohrid (**Fig. 7**). These observations suggest that for most  
568 of the Holocene Hg fluxes into the two lakes were largely decoupled, likely due to differences in  
569 catchment and basin dynamics which impacted the rate of Hg delivery to (and burial in) the lakes.

570 Divergent Hg signals in Lake Ohrid and Lake Prespa during this time may be linked to heightened  
571 wildfire frequency and/or intensity. Wildfires have the capacity to (in)directly release Hg from  
572 vegetation, and/or through associated changes in soil erosion. Proxy evidence alludes to interglacial  
573 conditions characterised by heightened seasonality, characterized by very warm, dry summers  
574 coupled with wet, mild winters, an overall increase in the prevalence of deciduous tree species  
575 (Cvetkoska et al., 2014; Panagiotopoulos, 2013); but also an increase in macro and microcharcoal  
576 concentrations in Lake Prespa (**Fig.7**; Panagiotopoulos et al. 2013). Large wildfires would have a  
577 broadly regional-scale impact which, given the close proximity of our two lakes, could theoretically  
578 produce a measurable Hg signal in both systems. However, more frequent and/or intense regional  
579 fires could also yield measurably different sedimentary Hg signals by their capacity to: (1) enhance  
580 surface run off without a corresponding increase in erosion and effectively reduce transport of  
581 catchment sourced, mineral-hosted Hg (Mataix-Solera et al., 2011; Shakesby, 2011); (2) enhance  
582 downstream transport of Hg released from burned soils and bound to fine and coarse particulate  
583 matter (Burke et al., 2010; Takenaka et al., 2021); and/or (3) release large quantities of Hg into the  
584 atmosphere following biomass combustion (Howard et al., 2019; Melendez-Perez et al., 2014;  
585 Roshan and Biswas, 2023). All three combine to generate impacts that may vary in significance owing  
586 to lake-specific differences in sedimentation, accumulation, and flux of materials to/from the lake.

587 An increase in wildfire activity also corresponds to a period of intensifying human influence in the  
588 region; predominantly in the form of land use change, agriculture, and animal husbandry (Cvetkoska  
589 et al., 2014; Masi et al., 2018; Panagiotopoulos et al., 2013; Rothacker et al., 2018; Thienemann et  
590 al., 2017; Wagner et al., 2009). Widespread mineral resource exploitation and metalworking on the  
591 Balkan peninsula is recorded as early as ~8 ka (Gajić-Kvaščev et al., 2012; Longman et al., 2018;  
592 Radivojević and Roberts, 2021; Schotsmans et al., 2022), and release of detrital Hg during cinnabar  
593 ore extraction and use of Hg in gold extraction (amalgamation) has been linked to pronounced Hg  
594 contamination in modern sedimentary units in the region (Covelli et al., 2001; Fitzgerald and Lamborg,



595 2013). Directly quantifying the influence of (hydro)climate- versus human-driven impacts on  
596 sedimentary Hg records presents a major challenge as these factors are interdependent.  
597 Nonetheless, these factors could produce a more measurable effect in lake systems with heightened  
598 sensitivity to changes in water, nutrient and pollutant fluxes. This could explain why large Hg signals  
599 are observed in Lake Prespa between ~12 and 3 ka but not Lake Ohrid: Lake Prespa is shallow  
600 relative to its surface area (**Fig. 2**), meaning that relatively small oscillations in pollutant influxes can  
601 lead to appreciable changes in lake geochemistry (Cvetkoska et al., 2015; Matzinger et al., 2006).

602 Decoupling of the two Hg records effectively disappears ~3 ka ago, where both lakes show a sharp  
603 and pronounced rise in Hg<sub>T</sub> and Hg<sub>AR</sub> (**Fig. 7**). Several lines of evidence point to human activity as the  
604 primary cause. On a local scale, a rapid increase in the biological productivity (eutrophication) of Lake  
605 Prespa since ~1.6 (±0.06) ka alludes to greater disturbance of catchment soils by agricultural  
606 practices, and eventually use of inorganic compounds such as pesticides and fertilizers (Aufgebauer  
607 et al., 2012; Cvetkoska et al., 2014; Krstić et al., 2012; Leng et al., 2013). Signals observed in **Figure**  
608 **7** may thus be a product of human-induced changes in organic or minerogenic material flux: each  
609 facilitating more efficient delivery of catchment-sourced Hg (Fitzgerald et al., 2005), and possibly also  
610 stimulating microbial Hg methylation within the sediment (Soerensen et al., 2016). On a broader scale  
611 peaks in Hg<sub>T</sub> and Hg<sub>AR</sub> correspond to a sustained rise in European and/or global Hg emissions, owing  
612 to increased deforestation, fossil fuel extraction and combustion, and intentional use of Hg for  
613 resource extraction/production (Outridge et al., 2018; United Nations Environment Programme, 2018).  
614 An increasing number of sedimentary archives record coeval Hg enrichments as early as ~3 ka ago  
615 (Biskaborn et al., 2021; Guédron et al., 2019; Li et al., 2020; Pan et al., 2020). The emergence of  
616 simultaneous Hg<sub>T</sub> and Hg<sub>AR</sub> peaks in Lakes Ohrid and Prespa following ~3 ka underscores the  
617 magnitude and global distribution of this change in Hg sources and emissions (**Fig. 7**), and point to a  
618 rise in Hg fluxes between 3 and 0 ka that was distinct enough to effectively overwhelm previously  
619 dominant natural drivers of Hg variability.

620

#### 621 **4.4. Key differences & implications**

622 The magnitude and expression of Hg signals recorded in Lake Prespa and Lake Ohrid are different in  
623 three aspects. First, the extent to which different host phases can (or cannot) explain time-varying  
624 patterns in Hg concentration differs between the two lakes. Although only a limited fraction of Hg  
625 variability in either record can be explained by availability of any single host phase, the low degree of  
626 covariance that we do observe points to organic material playing the most significant role as a Hg  
627 host in Lake Prespa. In contrast, Hg correlates most strongly with detrital minerals in Lake Ohrid over  
628 the same period (0-90 ka) (**Fig. 4**). The second difference is visible during the last glaciation (~35–12  
629 ka): in Lake Ohrid Hg concentrations peak during the LGM (35.8–12 ka), whereas Lake Prespa  
630 captures transient, high-amplitude peaks during deglaciation, starting ~15-kyr later (**Fig. 7**). The third  
631 difference is visible during the Holocene. The largest signals in the entire Lake Prespa record are  
632 observed between ~8 and 0 ka, whereas Hg concentrations do not increase in Lake Ohrid until ~2 ka.



633 These observations raise the question: *for two lakes located in such close geographical proximity and*  
634 *having experienced similar climate conditions, what may have caused such pronounced differences*  
635 *from ~35 ka (Fig. 2)?*

636 Differences in sediment composition, water balance, bathymetric structure, and catchment dynamics  
637 may all offer plausible explanations. Materials delivered to a large and/or deep lake (e.g., Lake Ohrid)  
638 would be distributed over a greater total area, and must travel notably farther to reach the coring site  
639 (Hinderer and Einsele, 2001). This would require a sufficiently large influx of Hg to produce a  
640 detectable signal, and is more likely to produce a sedimentary signal that is significantly smaller than  
641 the equivalent 'dose' delivered to a smaller and/or shallower lake (e.g., Lake Prespa); even if coring  
642 sites are equal distance from the shorelines of their respective basins. Lake Prespa also shows  
643 pronounced variability in lake water  $\delta^{18}\text{O}$  ( $\pm 6\text{‰}$ ) (Leng et al., 2010), frequent lake level fluctuations  
644 (Cvetkoska et al., 2015), and slower rates of biological recovery following abrupt disturbance  
645 compared to Lake Ohrid (Cvetkoska et al., 2016; Jovanovska et al., 2016), but also the most  
646 pronounced changes in the amplitude and frequency of peaks in  $\text{Hg}_T$  and  $\text{Hg}_{AR}$  (Fig. 7). Thus, shallow  
647 lakes are likely more sensitive to changes in erosion, nutrient status, hydrology, and potentially also  
648 changes in terrestrial Hg cycling.

649 The two records presented here highlight that Hg cycling in lacustrine environments is distinct from  
650 open marine systems. In marine systems, Hg fluxes can be broadly modulated by large-scale  
651 continental sediment (Fadina et al., 2019; Figueiredo et al., 2022; Kita et al., 2016) and/or  
652 atmospheric inputs (Chede et al., 2022), and Hg burial flux ultimately becomes more closely related to  
653 host-phase availability. Conversely, both Lake Prespa and Lake Ohrid highlight how the local basin  
654 and catchment characteristics both exert a key control on the delivery of Hg to lacustrine sediments,  
655 and reinforce how smaller, shallower lakes may be particularly sensitive recorders of transient  
656 changes in these fluxes.

657 Our observations highlight that multi-millennial lacustrine Hg records allow a different perspective of  
658 the Hg cycle compared to marine records, and, for example, may be used to infer how local, regional  
659 and global climatic conditions could have altered processes important to the terrestrial Hg cycle.  
660 Because lacustrine records are much better suited to recording smaller-scale processes it is also  
661 clear that extrapolating the (non-marine) Hg cycle response from a single lacustrine Hg record is  
662 challenging. For example, a single-core approach could produce a large degree of uncertainty owing  
663 to variable sediment focussing and catchment-sourced influx of organic and inorganic materials (Blais  
664 and Kalf, 1995; Engstrom and Rose, 2013; Engstrom and Wright, 1984). A valuable next step would  
665 be to apply a source-to-sink approach within a well-known lacustrine catchment and assess the extent  
666 to which Hg sedimentation is spatially heterogeneous within a lacustrine system, and whether multiple  
667 cores extracted from different locations within the same basin would yield markedly different Hg  
668 trends. Work of this nature would make great strides toward assessing how representative of  
669 variability in the local Hg cycle a single core is, and whether intra-basin fluctuations in sedimentation,  
670 resuspension, and erosion could translate to measurable changes in sedimentary Hg burial.



671 Past changes in environmental Hg availability inferred from sedimentary records have typically been  
672 examined (and presented) by normalizing Hg to a dominant host phase, often taken as organic matter  
673 (Fadina et al., 2019; Figueiredo et al., 2020; Grasby et al., 2019; Kita et al., 2016; Percival et al.,  
674 2015). However, availability of organic matter or other host phases that scavenge Hg here appear to  
675 represent just one of several processes governing Hg burial in lacustrine systems, and this process is  
676 very likely systematically less significant compared to marine records in lieu of changes in catchment  
677 and basin processes such as erosion, nutrient status, and hydrology (Outridge et al., 2019). Outside  
678 pre-industrial times (or periods without an overwhelming global Hg cycle perturbation; such as during  
679 LIP formation (Grasby et al., 2019)), a single common process/mechanism is therefore unlikely to  
680 produce a unanimous stratigraphic signal across all lakes or even for two adjacent lakes as shown in  
681 this study.

682

## 683 **6. Conclusions**

684 To better understand local and regional impact of climate, vegetation and catchment characteristics  
685 on lacustrine Hg records, we present two new high-resolution, Hg records for the last ~90 kyr from  
686 Lake Prespa and Lake Ohrid. The two records show some similarities but also distinct differences in  
687 the strength of the relationships between Hg, TOC, TS, and detrital minerals (K), with only a relatively  
688 small proportion of Hg variability attributable to host phase availability in each record. Our findings  
689 provide three valuable insights. First, that local sedimentary environment does influence Hg burial.  
690 Covariance with host phases accounts for a limited proportion of the observed variability, suggesting  
691 that many of the Hg<sub>T</sub> and Hg<sub>AR</sub> signals recorded in Lake Prespa and Lake Ohrid reflect net Hg input to  
692 the two lakes across timescales ranging from decades to multiple millennia. Second, Hg signals can  
693 reflect changes (and also differences) in catchment hydrology and structure. Despite their proximity,  
694 the magnitude and expression of the recorded signals are considerably different between Lake  
695 Prespa and Lake Ohrid, suggesting these inputs changed relative to sedimentary setting and in  
696 response to changing interactions between the two systems. Finally, regional-scale climate variability  
697 can measurably affect the Hg signals retained in lake sediments: both lakes Prespa and Ohrid  
698 showing changes in Hg concentration and accumulation corresponding to glacial (late Pleistocene)  
699 and interglacial (Holocene) climate conditions. It follows that local, regional, or global changes in  
700 climate or hydrological cycling capable of affecting mineral soils, (peri-)glacial features or fire regime  
701 in the lake catchment could all impact Hg fluxes. These findings prompt further examination of how  
702 orbital-scale climate variability (>10<sup>3</sup>-year timescales) may influence the terrestrial Hg cycle, not only  
703 to better resolve processes acting on single lacustrine and terrestrial successions, but also to identify  
704 which of these (local) processes could hold relevance for Hg cycling on a global scale.

705

706



## 707 Competing Interests

708 The corresponding author declares that none of the authors have any competing interests.

709

## 710 Acknowledgements

711 ARP, IMF, JF, and TAM acknowledge funding from European Research Council Consolidator Grant  
712 V-ECHO (ERC-2018-COG-818717-V-ECHO). ARP thanks Professor David Thomas and Mona  
713 Edwards (School of Geography, Oxford) for logistical assistance with sample transfer and storage. KP  
714 acknowledges funding from the German Research Foundation (DFG grant PA 2664/4-1). All authors  
715 thank members of the Scientific Collaboration on Past Speciation Conditions in Lake Ohrid  
716 (SCOPSCO), and the CRC 806 “*Our Way to Europe - Culture-Environment Interaction and Human*  
717 *Mobility in the Late Quaternary*” projects: for their efforts in producing the Lake Ohrid and Lake  
718 Prespa sediment successions, and making the data available for scientific use.

719

## 720 References Cited

- 721 Allard, J. L., Hughes, P. D., Woodward, J. C., Fink, D., Simon, K., and Wilcken, K. M.: Late Pleistocene glaciers in Greece: A  
722 new 36Cl chronology, *Quaternary Science Reviews*, 245, 106528, <https://doi.org/10.1016/j.quascirev.2020.106528>, 2020.
- 723 Allard, J. L., Hughes, P. D., and Woodward, J. C.: A radiometric dating revolution and the Quaternary glacial history of the  
724 Mediterranean mountains, *Earth-Science Reviews*, 223, 103844, <https://doi.org/10.1016/j.earscirev.2021.103844>, 2021.
- 725 Aufgebauer, A., Panagiotopoulos, K., Wagner, B., Schaebitz, F., Viehberg, F. A., Vogel, H., Zanchetta, G., Sulpizio, R., Leng,  
726 M. J., and Damaschke, M.: Climate and environmental change in the Balkans over the last 17 ka recorded in sediments from  
727 Lake Prespa (Albania/F.Y.R. of Macedonia/Greece), *Quaternary International*, 274, 122–135,  
728 <https://doi.org/10.1016/j.quaint.2012.02.015>, 2012.
- 729 Belmecheri, S., Namiotko, T., Robert, C., von Grafenstein, U., and Danielopol, D. L.: Climate controlled ostracod preservation  
730 in Lake Ohrid (Albania, Macedonia), *Palaeogeography, Palaeoclimatology, Palaeoecology*, 277, 236–245,  
731 <https://doi.org/10.1016/j.palaeo.2009.04.013>, 2009.
- 732 Benoit, J. M., Gilmour, C. C., Mason, R. P., and Heyes, A.: Sulfide controls on mercury speciation and bioavailability to  
733 methylating bacteria in sediment pore water, *Environmental Science and Technology*, 33, 1780,  
734 <https://doi.org/10.1021/es992007q>, 1999.
- 735 Biester, H., Pérez-Rodríguez, M., Gilfedder, B.-S., Martínez Cortizas, A., and Hermanns, Y.-M.: Solar irradiance and primary  
736 productivity controlled mercury accumulation in sediments of a remote lake in the Southern Hemisphere during the past 4000  
737 years: Primary productivity and mercury accumulation, *Limnol. Oceanogr.*, 63, 540–549, <https://doi.org/10.1002/lno.10647>,  
738 2018.
- 739 Bin, C., Xiaoru, W., and Lee, F. S. C.: Pyrolysis coupled with atomic absorption spectrometry for the determination of mercury  
740 in Chinese medicinal materials, *Analytica Chimica Acta*, 447, 161–169, [https://doi.org/10.1016/S0003-2670\(01\)01218-1](https://doi.org/10.1016/S0003-2670(01)01218-1), 2001.
- 741 Bishop, K., Shanley, J. B., Riscassi, A., de Wit, H. A., Eklöf, K., Meng, B., Mitchell, C., Osterwalder, S., Schuster, P. F.,  
742 Webster, J., and Zhu, W.: Recent advances in understanding and measurement of mercury in the environment: Terrestrial Hg  
743 cycling, *Science of the Total Environment*, 721, <https://doi.org/10.1016/j.scitotenv.2020.137647>, 2020.
- 744 Biskaborn, B. K., Narancic, B., Stoof-Leichsenring, K. R., Pestryakova, L. A., Appleby, P. G., Piliposian, G. T., and Diekmann,  
745 B.: Effects of climate change and industrialization on Lake Bolshoe Toko, eastern Siberia, *J Paleolimnol*, 65, 335–352,  
746 <https://doi.org/10.1007/s10933-021-00175-z>, 2021.
- 747 Blaauw, M. and Christeny, J. A.: Flexible paleoclimate age-depth models using an autoregressive gamma process, *Bayesian*  
748 *Analysis*, 6, 457–474, <https://doi.org/10.1214/11-BA618>, 2011.



- 749 Blais, J. M. and Kalf, J.: The influence of lake morphometry on sediment focusing, *Limnol. Oceanogr.*, 40, 582–588,  
750 <https://doi.org/10.4319/lo.1995.40.3.0582>, 1995.
- 751 Branfireun, B. A., Cosio, C., Poulain, A. J., Riise, G., and Bravo, A. G.: Mercury cycling in freshwater systems - An updated  
752 conceptual model, *Science of the Total Environment*, 745, <https://doi.org/10.1016/j.scitotenv.2020.140906>, 2020.
- 753 Burke, M. P., Hogue, T. S., Ferreira, M., Mendez, C. B., Navarro, B., Lopez, S., and Jay, J. A.: The Effect of Wildfire on Soil  
754 Mercury Concentrations in Southern California Watersheds, *Water Air Soil Pollut.*, 212, 369–385,  
755 <https://doi.org/10.1007/s11270-010-0351-y>, 2010.
- 756 Carrivick, J. L. and Tweed, F. S.: Deglaciation controls on sediment yield: Towards capturing spatio-temporal variability, *Earth-  
757 Science Reviews*, 221, 103809, <https://doi.org/10.1016/j.earscirev.2021.103809>, 2021.
- 758 Chakraborty, P., Sarkar, A., Vudamala, K., Naik, R., and Nath, B. N.: Organic matter - A key factor in controlling mercury  
759 distribution in estuarine sediment, *Marine Chemistry*, 173, 302–309, <https://doi.org/10.1016/j.marchem.2014.10.005>, 2015.
- 760 Chede, B. S., Venancio, I. M., Figueiredo, T. S., Albuquerque, A. L. S., and Silva-Filho, E. V.: Mercury deposition in the western  
761 tropical South Atlantic during the last 70 ka, *Palaeogeography, Palaeoclimatology, Palaeoecology*, 601, 111122,  
762 <https://doi.org/10.1016/j.palaeo.2022.111122>, 2022.
- 763 Cooke, C. A., Martínez-Cortizas, A., Bindler, R., and Sexauer Gustin, M.: Environmental archives of atmospheric Hg deposition  
764 – A review, *Science of the Total Environment*, 709, 134800, <https://doi.org/10.1016/j.scitotenv.2019.134800>, 2020.
- 765 Cordeiro, R. C., Turcq, B., Sifeddine, A., Lacerda, L. D., Silva Filho, E. V., Gueiros, B., Potty, Y. P., Santelli, R. E., Pádua, E.  
766 O., and Patchinelam, S. R.: Biogeochemical indicators of environmental changes from 50Ka to 10Ka in a humid region of the  
767 Brazilian Amazon, *Palaeogeography, Palaeoclimatology, Palaeoecology*, 299, 426–436,  
768 <https://doi.org/10.1016/j.palaeo.2010.11.021>, 2011.
- 769 Covelli, S., Faganeli, J., Horvat, M., and Brambati, A.: Mercury contamination of coastal sediments as the result of long-term  
770 cinnabar mining activity (Gulf of Trieste, northern Adriatic sea), *Applied Geochemistry*, 16, 541–558,  
771 [https://doi.org/10.1016/S0883-2927\(00\)00042-1](https://doi.org/10.1016/S0883-2927(00)00042-1), 2001.
- 772 Cvetkoska, A., Levkov, Z., Reed, J. M., and Wagner, B.: Late Glacial to Holocene climate change and human impact in the  
773 Mediterranean: The last ca. 17ka diatom record of Lake Prespa (Macedonia/Albania/Greece), *Palaeogeography,  
774 Palaeoclimatology, Palaeoecology*, 406, 22–32, <https://doi.org/10.1016/j.palaeo.2014.04.010>, 2014.
- 775 Cvetkoska, A., Levkov, Z., Reed, J. M., Wagner, B., Panagiotopoulos, K., Leng, M. J., and Lacey, J. H.: Quaternary climate  
776 change and Heinrich events in the southern Balkans: Lake Prespa diatom palaeolimnology from the last interglacial to present,  
777 *Journal of Paleolimnology*, 53, 215–231, <https://doi.org/10.1007/s10933-014-9821-3>, 2015.
- 778 Cvetkoska, A., Jovanovska, E., Francke, A., Tofilovska, S., Vogel, H., Levkov, Z., Donders, T. H., Wagner, B., and Wagner-  
779 Cremer, F.: Ecosystem regimes and responses in a coupled ancient lake system from MIS 5b to present: the diatom record of  
780 lakes Ohrid and Prespa, *Biogeosciences*, 13, 3147–3162, <https://doi.org/10.5194/bg-13-3147-2016>, 2016.
- 781 Damaschke, M., Sulpizio, R., Zanchetta, G., Wagner, B., Böhm, A., Nowaczyk, N., Rethemeyer, J., and Hilgers, A.:  
782 Tephrostratigraphic studies on a sediment core from Lake Prespa in the Balkans, *Climate of the Past*, 9, 267–287,  
783 <https://doi.org/10.5194/cp-9-267-2013>, 2013.
- 784 Ding, X., Li, D., Zheng, L., Bao, H., Chen, H.-F., and Kao, S.-J.: Sulfur Geochemistry of a Lacustrine Record from Taiwan  
785 Reveals Enhanced Marine Aerosol Input during the Early Holocene, *Sci Rep.*, 6, 38989, <https://doi.org/10.1038/srep38989>,  
786 2016.
- 787 Donders, T., Panagiotopoulos, K., Koutsodendris, A., Bertini, A., Mercuri, A. M., Masi, A., Combourieu-Nebout, N., Joannin, S.,  
788 Kouli, K., Kousis, I., Peyron, O., Torri, P., Florenzano, A., Francke, A., Wagner, B., and Sadori, L.: 1.36 million years of  
789 Mediterranean forest refugium dynamics in response to glacial-interglacial cycle strength, *Proceedings of the National  
790 Academy of Sciences of the United States of America*, 118, <https://doi.org/10.1073/pnas.2026111118>, 2021.
- 791 Driscoll, C. T., Mason, R. P., Chan, H. M., Jacob, D. J., and Pirrone, N.: Mercury as a global pollutant: Sources, pathways, and  
792 effects, *Environmental Science and Technology*, 47, 4967–4983, <https://doi.org/10.1021/es305071v>, 2013.
- 793 Durnford, D. and Dastoor, A.: The behavior of mercury in the cryosphere: A review of what we know from observations, *Journal  
794 of Geophysical Research Atmospheres*, 116, <https://doi.org/10.1029/2010JD014809>, 2011.
- 795 Edwards, B. A., Kushner, D. S., Outridge, P. M., and Wang, F.: Fifty years of volcanic mercury emission research: Knowledge  
796 gaps and future directions, *Science of the Total Environment*, 757, 143800, <https://doi.org/10.1016/j.scitotenv.2020.143800>,  
797 2021.
- 798 Eftimi, R., Skende, P., and Zoto, J.: An isotope study of the connection of Ohrid and Prespa lakes, *Geologica Balcanica*, 32,  
799 43–49, 1999.



- 800 Ehrmann, W. and Schmiedl, G.: Nature and dynamics of North African humid and dry periods during the last 200,000 years  
801 documented in the clay fraction of eastern mediterranean deep-sea sediments, *Quaternary Science Reviews*, 260, 106925,  
802 <https://doi.org/10.1016/j.quascirev.2021.106925>, 2021.
- 803 Engstrom, D. R. and Rose, N. L.: A whole-basin, mass-balance approach to paleolimnology, *J Paleolimnol*, 49, 333–347,  
804 <https://doi.org/10.1007/s10933-012-9675-5>, 2013.
- 805 Engstrom, D. R. and Wright, H. E.: Chemical stratigraphy of lake sediments as a record of environmental change, in: *Lake  
806 Sediments and Environmental History*, University of Minnesota Press, 11–67, 1984.
- 807 Fadina, O. A., Venancio, I. M., Belem, A., Silveira, C. S., Bertagnolli, D. de C., Silva-Filho, E. V., and Albuquerque, A. L. S.:  
808 Paleoclimatic controls on mercury deposition in northeast Brazil since the Last Interglacial, *Quaternary Science Reviews*, 221,  
809 105869, <https://doi.org/10.1016/j.quascirev.2019.105869>, 2019.
- 810 Figueiredo, T. S., Santos, T. P., Costa, K. B., Toledo, F., Albuquerque, A. L. S., Smoak, J. M., Bergquist, B. A., and Silva-Filho,  
811 E. V.: Effect of deep Southwestern Subtropical Atlantic Ocean circulation on the biogeochemistry of mercury during the last two  
812 glacial/interglacial cycles, *Quaternary Science Reviews*, 239, 106368, <https://doi.org/10.1016/j.quascirev.2020.106368>, 2020.
- 813 Figueiredo, T. S., Bergquist, B. A., Santos, T. P., Albuquerque, A. L. S., and Silva-Filho, E. V.: Relationship between glacial  
814 CO<sub>2</sub> drawdown and mercury cycling in the western South Atlantic: An isotopic insight, *Geology*, 50, 3–7,  
815 <https://doi.org/10.1130/g49942.1>, 2022.
- 816 Fitzgerald, W. F. and Lamborg, C. H.: *Geochemistry of Mercury in the Environment*, Elsevier Ltd., 91–129 pp.,  
817 <https://doi.org/10.1016/B978-0-08-095975-7.00904-9>, 2013.
- 818 Fitzgerald, W. F., Engstrom, D. R., Lamborg, C. H., Tseng, C.-M., Balcom, P. H., and Hammerschmidt, C. R.: Modern and  
819 Historic Atmospheric Mercury Fluxes in Northern Alaska: Global Sources and Arctic Depletion, *Environ. Sci. Technol.*, 39, 557–  
820 568, <https://doi.org/10.1021/es049128x>, 2005.
- 821 Francke, A., Wagner, B., Just, J., Leicher, N., Gromig, R., Baumgarten, H., Vogel, H., Lacey, J. H., Sadori, L., Wonik, T., Leng,  
822 M. J., Zanchetta, G., Sulpizio, R., and Giaccio, B.: Sedimentological processes and environmental variability at Lake Ohrid  
823 (Macedonia, Albania) between 637 ka and the present, *Biogeosciences*, 13, 1179–1196, [https://doi.org/10.5194/bg-13-1179-](https://doi.org/10.5194/bg-13-1179-2016)  
824 2016, 2016.
- 825 Francke, A., Dosseto, A., Panagiotopoulos, K., Leicher, N., Lacey, J. H., Kyrikou, S., Wagner, B., Zanchetta, G., Kouli, K., and  
826 Leng, M. J.: Sediment residence time reveals Holocene shift from climatic to vegetation control on catchment erosion in the  
827 Balkans, *Global and Planetary Change*, 177, 186–200, <https://doi.org/10.1016/j.gloplacha.2019.04.005>, 2019.
- 828 Frieling, J., Mather, T. A., März, C., Jenkyns, H. C., Hennekam, R., Reichart, G.-J., Slomp, C. P., and Van Helmond, N. A. G.  
829 M.: Effects of redox variability and early diagenesis on marine sedimentary Hg records, *Geochimica et Cosmochimica Acta*,  
830 S0016703723001850, <https://doi.org/10.1016/j.gca.2023.04.015>, 2023.
- 831 Gajić-Kvaščev, M., Stojanović, M. M., Šmit, Ž., Kantarelou, V., Karydas, A. G., Šljivar, D., Milovanović, D., and Andrić, V.: New  
832 evidence for the use of cinnabar as a colouring pigment in the Vinča culture, *Journal of Archaeological Science*, 39, 1025–  
833 1033, <https://doi.org/10.1016/j.jas.2011.11.023>, 2012.
- 834 Garcia-Ordiales, E., Covelli, S., Rico, J. M., Roqueñí, N., Fontolan, G., Flor-Blanco, G., Cienfuegos, P., and Loredó, J.:  
835 Occurrence and speciation of arsenic and mercury in estuarine sediments affected by mining activities (Asturias, northern  
836 Spain), *Chemosphere*, 198, 281–289, <https://doi.org/10.1016/j.chemosphere.2018.01.146>, 2018.
- 837 Gelety, V. F., Kalmykov, G. V., and Parkhomenko, I. Y.: Mercury in the sedimentary deposits of Lake Baikal, *Geochemistry  
838 International*, 45, 170–177, <https://doi.org/10.1134/S001670290702005X>, 2007.
- 839 Giaccio, B., Hajdas, I., Isaia, R., Deino, A., and Nomade, S.: High-precision <sup>14</sup>C and <sup>40</sup>Ar/<sup>39</sup>Ar dating of the Campanian  
840 Ignimbrite (Y-5) reconciles the time-scales of climatic-cultural processes at 40 ka, *Scientific Reports*, 7, 1–10,  
841 <https://doi.org/10.1038/srep45940>, 2017.
- 842 Goosse, H., Brovkin, V., Fichefet, T., Haarsma, R., Huybrechts, P., Jongma, J., Mouchet, A., Selten, F., Barriat, P. Y., Campin,  
843 J. M., Deleersnijder, E., Driesschaert, E., Goelzer, H., Janssens, I., Loutre, M. F., Morales Maqueda, M. A., Opsteegh, T.,  
844 Mathieu, P. P., Munhoven, G., Pettersson, E. J., Renssen, H., Roche, D. M., Schaeffer, M., Tartinville, B., Timmermann, A.,  
845 and Weber, S. L.: Description of the Earth system model of intermediate complexity LOVECLIM version 1.2, *Geoscientific  
846 Model Development*, 3, 603–633, <https://doi.org/10.5194/gmd-3-603-2010>, 2010.
- 847 Grasby, S. E., Them, T. R., Chen, Z., Yin, R., and Ardakani, O. H.: Mercury as a proxy for volcanic emissions in the geologic  
848 record, *Earth-Science Reviews*, 196, 102880, <https://doi.org/10.1016/j.earscirev.2019.102880>, 2019.
- 849 Gromig, R., Mechernich, S., Ribolini, A., Wagner, B., Zanchetta, G., Isola, I., Bini, M., and Dunai, T. J.: Evidence for a Younger  
850 Dryas deglaciation in the Galicica Mountains (FYROM) from cosmogenic <sup>36</sup>Cl, *Quaternary International*, 464, 352–363,  
851 <https://doi.org/10.1016/j.quaint.2017.07.013>, 2018.



- 852 Grygar, T. M., Mach, K., and Martinez, M.: Checklist for the use of potassium concentrations in siliciclastic sediments as  
853 paleoenvironmental archives, *Sedimentary Geology*, 382, 75–84, <https://doi.org/10.1016/j.sedgeo.2019.01.010>, 2019.
- 854 Guédron, S., Tolu, J., Brisset, E., Sabatier, P., Perrot, V., Bouchet, S., Develle, A. L., Bindler, R., Cossa, D., Fritz, S. C., and  
855 Baker, P. A.: Late Holocene volcanic and anthropogenic mercury deposition in the western Central Andes (Lake Chungará  
856 Chile), *Science of the Total Environment*, 662, 903–914, <https://doi.org/10.1016/j.scitotenv.2019.01.294>, 2019.
- 857 Han, S., Obraztsova, A., Pretto, P., Deheyn, D. D., Gieskes, J., and Tebo, B. M.: Sulfide and iron control on mercury speciation  
858 in anoxic estuarine sediment slurries, *Marine Chemistry*, 111, 214–220, <https://doi.org/10.1016/j.marchem.2008.05.002>, 2008.
- 859 Hinderer, M. and Einsele, G.: The world's large lake basins as denudation-accumulation systems and implications for their  
860 lifetimes, *Journal of Paleolimnology*, 26, 355–372, 2001.
- 861 Hollis, G. E. and Stevenson, A. C.: The physical basis of the Lake Mikri Prespa systems: Geology, climate, hydrology and water  
862 quality, *Hydrobiologia*, 351, 1–19, <https://doi.org/10.1023/A:1003067115862>, 1997.
- 863 Holmer, M. and Storkholm, P.: Sulphate reduction and sulphur cycling in lake sediments: a review: Sulphate cycling in lake  
864 sediments, *Freshwater Biology*, 46, 431–451, <https://doi.org/10.1046/j.1365-2427.2001.00687.x>, 2001.
- 865 Howard, D., Macsween, K., Edwards, G. C., Desservettaz, M., Guérette, E. A., Paton-Walsh, C., Surawski, N. C., Sullivan, A.  
866 L., Weston, C., Volkova, L., Powell, J., Keywood, M. D., Reisen, F., and (Mick) Meyer, C. P.: Investigation of mercury emissions  
867 from burning of Australian eucalypt forest surface fuels using a combustion wind tunnel and field observations, *Atmospheric  
868 Environment*, 202, 17–27, <https://doi.org/10.1016/j.atmosenv.2018.12.015>, 2019.
- 869 Hughes, P. D. and Woodward, J. C.: Quaternary glaciation in the Mediterranean mountains: A new synthesis, *Geological  
870 Society Special Publication*, 433, 1–23, <https://doi.org/10.1144/SP433.14>, 2017.
- 871 Hughes, P. D., Woodward, J. C., Gibbard, P. L., Macklin, M. G., Gilmour, M. A., and Smith, G. R.: The glacial history of the  
872 Pindus Mountains, Greece, *Journal of Geology*, 114, 413–434, <https://doi.org/10.1086/504177>, 2006.
- 873 Hughes, P. D., Allard, J. L., and Woodward, J. C.: The Balkans: glacial landforms prior to the Last Glacial Maximum, *European  
874 Glacial Landscapes*, 323–332, <https://doi.org/10.1016/b978-0-12-823498-3.00034-0>, 2022.
- 875 Hughes, P. D., Allard, J. L., Woodward, J. C., and Pope, R. J. J.: The Balkans: glacial landforms during deglaciation, in:  
876 *European Glacial Landscapes*, Elsevier, 221–231, <https://doi.org/10.1016/B978-0-323-91899-2.00055-3>, 2023.
- 877 Jitaru, P., Gabrielli, P., Marteel, A., Plane, J. M. C., Planchon, F. A. M., Gauchard, P. A., Ferrari, C. P., Boutron, C. F., Adams,  
878 F. C., Hong, S., Cescon, P., and Barbante, C.: Atmospheric depletion of mercury over Antarctica during glacial periods, *Nature  
879 Geoscience*, 2, 505–508, <https://doi.org/10.1038/ngeo549>, 2009.
- 880 Jovanovska, E., Cvetkoska, A., Hauffe, T., Levkov, Z., Wagner, B., Sulpizio, R., Francke, A., Albrecht, C., and Wilke, T.:  
881 Differential resilience of ancient sister lakes Ohrid and Prespa to environmental disturbances during the Late Pleistocene,  
882 *Biogeosciences*, 13, 1149–1161, <https://doi.org/10.5194/bg-13-1149-2016>, 2016.
- 883 Just, J., Nowaczyk, N., Francke, A., Sagnotti, L., and Wagner, B.: Climatic control on the occurrence of high-coercivity magnetic  
884 minerals and preservation of greigite in a 640 ka sediment sequence from Lake Ohrid (Balkans), *Biogeosciences Discussions*,  
885 12, 14215–14243, <https://doi.org/10.5194/bgd-12-14215-2015>, 2015.
- 886 Kita, I., Yamashita, T., Chiyonobu, S., Hasegawa, H., Sato, T., and Kuwahara, Y.: Mercury content in Atlantic sediments as a  
887 new indicator of the enlargement and reduction of Northern Hemisphere ice sheets, *Journal of Quaternary Science*, 31, 167–  
888 177, <https://doi.org/10.1002/jqs.2854>, 2016.
- 889 Kohler, S. G., Petrova, M. V., Digernes, M. G., Sanchez, N., Dufour, A., Simić, A., Ndungu, K., and Ardelan, M. V.: Arctic  
890 Ocean's wintertime mercury concentrations limited by seasonal loss on the shelf, *Nature Geoscience*,  
891 <https://doi.org/10.1038/s41561-022-00986-3>, 2022.
- 892 Kongchum, M., Hudnall, W. H., and Delaune, R. D.: Relationship between sediment clay minerals and total mercury, *Journal of  
893 Environmental Science and Health - Part A Toxic/Hazardous Substances and Environmental Engineering*, 46, 534–539,  
894 <https://doi.org/10.1080/10934529.2011.551745>, 2011.
- 895 Krstić, S., Zdraveski, N., and Blinkova, M.: Implementing the WFD in River Basin Management Plans – A Case Study of Prespa  
896 Lake Watershed, in: BALWOIS, 2012.
- 897 de Lacerda, L. D., Turcq, B., Sifeddine, A., and Cordeiro, R. C.: Mercury accumulation rates in Caço Lake, NE Brazil during the  
898 past 20,000 years, *Journal of South American Earth Sciences*, 77, 42–50, <https://doi.org/10.1016/j.jsames.2017.04.008>, 2017.
- 899 Lacey, J. H. and Jones, M. D.: Quantitative reconstruction of early Holocene and last glacial climate on the Balkan Peninsula  
900 using coupled hydrological and isotope mass balance modelling, *Quaternary Science Reviews*, 202, 109–121,  
901 <https://doi.org/10.1016/j.quascirev.2018.09.007>, 2018.



- 902 Lacey, J. H., Leng, M. J., Francke, A., Sloane, H. H., Milodowski, A., Vogel, H., Baumgarten, H., Zanchetta, G., and Wagner,  
903 B.: Northern Mediterranean climate since the Middle Pleistocene: A 637 ka stable isotope record from Lake Ohrid  
904 (Albania/Macedonia), *Biogeosciences*, 13, 1801–1820, <https://doi.org/10.5194/bg-13-1801-2016>, 2016.
- 905 Leicher, N., Giaccio, B., Zanchetta, G., Sulpizio, R., Albert, P. G., Tomlinson, E. L., Lagos, M., Francke, A., and Wagner, B.:  
906 Lake Ohrid's tephrochronological dataset reveals 1.36 Ma of Mediterranean explosive volcanic activity, *Scientific Data*, 8, 1–14,  
907 <https://doi.org/10.1038/s41597-021-01013-7>, 2021.
- 908 Leng, M. J., Baneschi, I., Zanchetta, G., Jex, C. N., Wagner, B., and Vogel, H.: Late Quaternary palaeoenvironmental  
909 reconstruction from Lakes Ohrid and Prespa (Macedonia/Albania border) using stable isotopes, *Biogeosciences*, 7, 3109–3122,  
910 <https://doi.org/10.5194/bg-7-3109-2010>, 2010.
- 911 Leng, M. J., Wagner, B., Boehm, A., Panagiotopoulos, K., Vane, C. H., Snelling, A., Haidon, C., Woodley, E., Vogel, H.,  
912 Zanchetta, G., and Baneschi, I.: Understanding past climatic and hydrological variability in the mediterranean from Lake Prespa  
913 sediment isotope and geochemical record over the last glacial cycle, *Quaternary Science Reviews*, 66, 123–136,  
914 <https://doi.org/10.1016/j.quascirev.2012.07.015>, 2013.
- 915 Leontaritis, A. D., Kouli, K., and Pavlopoulos, K.: The glacial history of Greece: a comprehensive review, *Mediterranean  
916 Geoscience Reviews*, 2, 65–90, <https://doi.org/10.1007/s42990-020-00021-w>, 2020.
- 917 Lewin, J., Macklin, M. G., and Woodward, J. C.: Late quaternary fluvial sedimentation in the voidomatis basin, Epirus,  
918 Northwest Greece, *Quaternary Research*, 35, 103–115, [https://doi.org/10.1016/0033-5894\(91\)90098-P](https://doi.org/10.1016/0033-5894(91)90098-P), 1991.
- 919 Lézine, A. M., von Grafenstein, U., Andersen, N., Belmecheri, S., Bordon, A., Caron, B., Cazet, J. P., Erlenkeuser, H.,  
920 Fouache, E., Grenier, C., Huntsman-Mapila, P., Hureau-Mazaudier, D., Manelli, D., Mazaud, A., Robert, C., Sulpizio, R.,  
921 Tiercelin, J. J., Zanchetta, G., and Zeqollari, Z.: Lake Ohrid, Albania, provides an exceptional multi-proxy record of  
922 environmental changes during the last glacial-interglacial cycle, *Palaeogeography, Palaeoclimatology, Palaeoecology*, 287,  
923 116–127, <https://doi.org/10.1016/j.palaeo.2010.01.016>, 2010.
- 924 Li, C., Enrico, M., Magand, O., Araujo, B. F., Le Roux, G., Osterwalder, S., Dommergue, A., Bertrand, Y., Brioude, J., De  
925 Vleeschouwer, F., and Sonke, J. E.: A peat core Hg stable isotope reconstruction of Holocene atmospheric Hg deposition at  
926 Amsterdam Island (37.8oS), *Geochimica et Cosmochimica Acta*, 341, 62–74, <https://doi.org/10.1016/j.gca.2022.11.024>, 2023.
- 927 Li, F., Ma, C., and Zhang, P.: Mercury Deposition, Climate Change and Anthropogenic Activities: A Review, *Frontiers in Earth  
928 Science*, 8, <https://doi.org/10.3389/feart.2020.00316>, 2020.
- 929 Lindhorst, K., Krastel, S., Reichert, K., Stipp, M., Wagner, B., and Schwenk, T.: Sedimentary and tectonic evolution of Lake  
930 Ohrid (Macedonia/Albania), *Basin Res.*, 27, 84–101, <https://doi.org/10.1111/bre.12063>, 2015.
- 931 Lisiecki, L. E. and Raymo, M. E.: A Pliocene-Pleistocene stack of 57 globally distributed benthic  $\delta^{18}\text{O}$  records,  
932 *Paleoceanography*, 20, 1–17, <https://doi.org/10.1029/2004PA001071>, 2005.
- 933 Longman, J., Veres, D., Finsinger, W., and Ersek, V.: Exceptionally high levels of lead pollution in the Balkans from the Early  
934 Bronze Age to the Industrial Revolution, *Proc. Natl. Acad. Sci. U.S.A.*, 115, <https://doi.org/10.1073/pnas.1721546115>, 2018.
- 935 Lyman, S. N., Cheng, I., Gratz, L. E., Weiss-Penzias, P., and Zhang, L.: An updated review of atmospheric mercury, *Science of  
936 the Total Environment*, 707, 135575, <https://doi.org/10.1016/j.scitotenv.2019.135575>, 2020.
- 937 Masi, A., Francke, A., Pepe, C., Thienemann, M., Wagner, B., and Sadori, L.: Vegetation history and paleoclimate at Lake  
938 Dojran (FYROM/Greece) during the Late Glacial and Holocene, *Clim. Past*, 14, 351–367, <https://doi.org/10.5194/cp-14-351-2018>, 2018.
- 940 Mataix-Solera, J., Cerdà, A., Arcenegui, V., Jordán, A., and Zavala, L. M.: Fire effects on soil aggregation: A review, *Earth-  
941 Science Reviews*, 109, 44–60, <https://doi.org/10.1016/j.earscirev.2011.08.002>, 2011.
- 942 Matzinger, A., Jordanoski, M., Veljanoska-Sarafiloska, E., Sturm, M., Müller, B., and Wüest, A.: Is Lake Prespa jeopardizing the  
943 ecosystem of ancient Lake Ohrid?, *Hydrobiologia*, 553, 89–109, <https://doi.org/10.1007/s10750-005-6427-9>, 2006.
- 944 Melendez-Perez, J. J., Fostier, A. H., Carvalho, J. A., Windmöller, C. C., Santos, J. C., and Carpi, A.: Soil and biomass mercury  
945 emissions during a prescribed fire in the Amazonian rain forest, *Atmospheric Environment*, 96, 415–422,  
946 <https://doi.org/10.1016/j.atmosenv.2014.06.032>, 2014.
- 947 Nasr, M., Ogilvie, J., Castonguay, M., Rencz, A., and Arp, P. A.: Total Hg concentrations in stream and lake sediments:  
948 Discerning geospatial patterns and controls across Canada, *Applied Geochemistry*, 26, 1818–1831,  
949 <https://doi.org/10.1016/j.apgeochem.2011.06.006>, 2011.
- 950 Oliva, M., Žebre, M., Guglielmin, M., Hughes, P. D., Çiner, A., Vieira, G., Bodin, X., Andrés, N., Colucci, R. R., García-  
951 Hernández, C., Mora, C., Nofre, J., Palacios, D., Pérez-Alberti, A., Ribolini, A., Ruiz-Fernández, J., Sarkaya, M. A., Serrano,  
952 E., Urdea, P., Valcárcel, M., Woodward, J. C., and Yıldırım, C.: Permafrost conditions in the Mediterranean region since the  
953 Last Glaciation, *Earth-Science Reviews*, 185, 397–436, <https://doi.org/10.1016/j.earscirev.2018.06.018>, 2018.



- 954 Outridge, Sanei, H., Stern, Hamilton, and Goodarzi, F.: Evidence for Control of Mercury Accumulation Rates in Canadian High  
955 Arctic Lake Sediments by Variations of Aquatic Primary Productivity, *Environ. Sci. Technol.*, 41, 5259–5265,  
956 <https://doi.org/10.1021/es070408x>, 2007.
- 957 Outridge, P. M., Mason, R. P., Wang, F., Guerrero, S., and Heimbürger-Boavida, L. E.: Updated Global and Oceanic Mercury  
958 Budgets for the United Nations Global Mercury Assessment 2018, *Environmental Science and Technology*, 52, 11466–11477,  
959 <https://doi.org/10.1021/acs.est.8b01246>, 2018.
- 960 Outridge, P. M., Stern, G. A., Hamilton, P. B., and Sanei, H.: Algal scavenging of mercury in preindustrial Arctic lakes, *Limnol  
961 Oceanogr.*, 64, 1558–1571, <https://doi.org/10.1002/lno.11135>, 2019.
- 962 Overeem, I., Hudson, B. D., Syvitski, J. P. M., Mikkelsen, A. B., Hasholt, B., Van Den Broeke, M. R., Noel, B. P. Y., and  
963 Morlighem, M.: Substantial export of suspended sediment to the global oceans from glacial erosion in Greenland, *Nature  
964 Geoscience*, 10, 859–863, <https://doi.org/10.1038/NNGEO3046>, 2017.
- 965 Pan, J., Zhong, W., Wei, Z., Ouyang, J., Shang, S., Ye, S., Chen, Y., Xue, J., and Tang, X.: A 15,400-year record of natural and  
966 anthropogenic input of mercury (Hg) in a sub-alpine lacustrine sediment succession from the western Nanling Mountains, South  
967 China, *Environmental Science and Pollution Research*, 27, 20478–20489, <https://doi.org/10.1007/s11356-020-08421-z>, 2020.
- 968 Panagiotopoulos, K.: Late Quaternary ecosystem and climate interactions in SW Balkans inferred from Lake Prespa sediments,  
969 Universität zu Köln, Cologne, Germany, 2013.
- 970 Panagiotopoulos, K., Aufgebauer, A., Schäbitz, F., and Wagner, B.: Vegetation and climate history of the Lake Prespa region  
971 since the Lateglacial, *Quaternary International*, 293, 157–169, <https://doi.org/10.1016/j.quaint.2012.05.048>, 2013.
- 972 Panagiotopoulos, K., Böhm, A., Leng, M. J., Wagner, B., and Schäbitz, F.: Climate variability over the last 92 ka in SW Balkans  
973 from analysis of sediments from Lake Prespa, *Climate of the Past*, 10, 643–660, <https://doi.org/10.5194/cp-10-643-2014>, 2014.
- 974 Panagiotopoulos, K., Holtvoeth, J., Kouli, K., Marinova, E., Francke, A., Cvetkoska, A., Jovanovska, E., Lacey, J. H., Lyons, E.  
975 T., Buckel, C., Bertini, A., Donders, T., Just, J., Leicher, N., Leng, M. J., Melles, M., Pancost, R. D., Sadori, L., Tauber, P.,  
976 Vogel, H., Wagner, B., and Wilke, T.: Insights into the evolution of the young Lake Ohrid ecosystem and vegetation succession  
977 from a southern European refugium during the Early Pleistocene, *Quaternary Science Reviews*, 227,  
978 <https://doi.org/10.1016/j.quascirev.2019.106044>, 2020.
- 979 Percival, L. M. E., Witt, M. L. I., Mather, T. A., Hermoso, M., Jenkyns, H. C., Hesselbo, S. P., Al-Suwaidi, A. H., Storm, M. S.,  
980 Xu, W., and Ruhl, M.: Globally enhanced mercury deposition during the end-Pliensbachian extinction and Toarcian OAE: A link  
981 to the Karoo-Ferrar Large Igneous Province, *Earth and Planetary Science Letters*, 428, 267–280,  
982 <https://doi.org/10.1016/j.epsl.2015.06.064>, 2015.
- 983 Percival, L. M. E., Jenkyns, H. C., Mather, T. A., Dickson, A. J., Batenburg, S. J., Ruhl, M., Hesselbo, S. P., Barclay, R., Jarvis,  
984 I., Robinson, S. A., and Woelders, L.: Does large igneous province volcanism always perturb the mercury cycle? Comparing  
985 the records of Oceanic Anoxic Event 2 and the end-cretaceous to other Mesozoic events, *American Journal of Science*, 318,  
986 799–860, <https://doi.org/10.2475/08.2018.01>, 2018.
- 987 Pérez-Rodríguez, M., Horák-Terra, I., Rodríguez-Lado, L., Aboal, J. R., and Martínez Cortizas, A.: Long-Term (~57 ka) controls  
988 on mercury accumulation in the southern hemisphere reconstructed using a peat record from pinheiro mire (minas gerais,  
989 Brazil), *Environmental Science and Technology*, 49, 1356–1364, <https://doi.org/10.1021/es504826d>, 2015.
- 990 Pérez-Rodríguez, M., Margalef, O., Corella, J. P., Saiz-Lopez, A., Pla-Rabes, S., Giral, S., and Cortizas, A. M.: The role of  
991 climate: 71 ka of atmospheric mercury deposition in the southern hemisphere recorded by Rano Aroi Mire, Easter Island  
992 (Chile), *Geosciences (Switzerland)*, 8, <https://doi.org/10.3390/geosciences8100374>, 2018.
- 993 Pope, R. J., Hughes, P. D., and Skourtsos, E.: Glacial history of Mt Chelmos, Peloponnesus, Greece, *Geological Society  
994 Special Publication*, 433, 211–236, <https://doi.org/10.1144/SP433.11>, 2017.
- 995 Radivojević, M. and Roberts, B. W.: Early Balkan Metallurgy: Origins, Evolution and Society, 6200–3700 BC, Springer US,  
996 195–278 pp., <https://doi.org/10.1007/s10963-021-09155-7>, 2021.
- 997 Rasmussen, S. O., Bigler, M., Blockley, S. P., Blunier, T., Buchardt, S. L., Clausen, H. B., Cvijanovic, I., Dahl-Jensen, D.,  
998 Johnsen, S. J., Fischer, H., Gkinis, V., Guillevic, M., Hoek, W. Z., Lowe, J. J., Pedro, J. B., Popp, T., Seierstad, I. K.,  
999 Steffensen, J. P., Svensson, A. M., Vallenga, P., Vinther, B. M., Walker, M. J. C., Wheatley, J. J., and Winstrup, M.: A  
1000 stratigraphic framework for abrupt climatic changes during the Last Glacial period based on three synchronized Greenland ice-  
1001 core records: Refining and extending the INTIMATE event stratigraphy, *Quaternary Science Reviews*, 106, 14–28,  
1002 <https://doi.org/10.1016/j.quascirev.2014.09.007>, 2014.
- 1003 Ravichandran, M.: Interactions between mercury and dissolved organic matter - A review, *Chemosphere*, 55, 319–331,  
1004 <https://doi.org/10.1016/j.chemosphere.2003.11.011>, 2004.
- 1005 Reimer, P. J., Austin, W. E. N., Bard, E., Bayliss, A., Blackwell, P. G., Bronk Ramsey, C., Butzin, M., Cheng, H., Edwards, R.  
1006 L., Friedrich, M., Grootes, P. M., Guilderson, T. P., Hajdas, I., Heaton, T. J., Hogg, A. G., Hughen, K. A., Kromer, B., Manning,



- 1007 S. W., Muscheler, R., Palmer, J. G., Pearson, C., Van Der Plicht, J., Reimer, R. W., Richards, D. A., Scott, E. M., Southon, J.  
1008 R., Turney, C. S. M., Wacker, L., Adolphi, F., Büntgen, U., Capano, M., Fahrni, S. M., Fogtmann-Schulz, A., Friedrich, R.,  
1009 Köhler, P., Kudsk, S., Miyake, F., Olsen, J., Reinig, F., Sakamoto, M., Sookdeo, A., and Talamo, S.: The IntCal20 Northern  
1010 Hemisphere Radiocarbon Age Calibration Curve (0-55 cal kBP), *Radiocarbon*, 62, 725–757,  
1011 <https://doi.org/10.1017/RDC.2020.41>, 2020.
- 1012 Ribolini, A., Isola, I., Zanchetta, G., Bini, M., and Sulpizio, R.: Glacial features on the Galicica Mountains, Macedonia:  
1013 Preliminary report, *Geografia Fisica e Dinamica Quaternaria*, 34, 247–255, <https://doi.org/10.4461/GFDQ.2011.34.22>, 2011.
- 1014 Ribolini, A., Bini, M., Isola, I., Spagnolo, M., Zanchetta, G., Pellitero, R., Mechernich, S., Gromig, R., Dunai, T., Wagner, B., and  
1015 Milevski, I.: An oldest dryas glacier expansion on mount pelister (former Yugoslavian Republic of Macedonia) according to  
1016  $^{10}\text{Be}$  cosmogenic dating, *Journal of the Geological Society*, 175, 100–110, <https://doi.org/10.1144/jgs2017-038>, 2018.
- 1017 Roshan, A. and Biswas, A.: Fire-induced geochemical changes in soil: Implication for the element cycling, *Science of The Total  
1018 Environment*, 868, 161714, <https://doi.org/10.1016/j.scitotenv.2023.161714>, 2023.
- 1019 Rothacker, L., Dosseto, A., Francke, A., Chivas, A. R., Vigier, N., Kotarba-Morley, A. M., and Menozzi, D.: Impact of climate  
1020 change and human activity on soil landscapes over the past 12,300 years, *Sci Rep*, 8, 247, <https://doi.org/10.1038/s41598-017-18603-4>, 2018.
- 1022 Ruszkiczay-Rüdiger, Z., Kern, Z., Temovski, M., Madarász, B., Milevski, I., and Braucher, R.: Last deglaciation in the central  
1023 Balkan Peninsula: Geochronological evidence from the Jablanica Mt. (North Macedonia), *Geomorphology*, 351,  
1024 <https://doi.org/10.1016/j.geomorph.2019.106985>, 2020.
- 1025 Rytuba, J. J.: Mercury from mineral deposits and potential environmental impact, *Environmental Geology*, 43, 326–338,  
1026 <https://doi.org/10.1007/s00254-002-0629-5>, 2003.
- 1027 Sadori, L., Koutsodendris, A., Panagiotopoulos, K., Masi, A., Bertini, A., Combourieu-Nebout, N., Francke, A., Kouli, K., Kousis,  
1028 I., Joannin, S., Maria Mercuri, A., Peyron, O., Torri, P., Wagner, B., Zanchetta, G., Sinopoli, G., and Donders, T. H.:  
1029 Corrigendum to “Pollen-based paleoenvironmental and paleoclimatic change at Lake Ohrid (south-eastern Europe) during the  
1030 past 500 ka,” *Biogeosciences*, 13, 1423–1427, <https://doi.org/10.5194/bg-13-1423-2016-corrigendum>, 2016a.
- 1031 Sadori, L., Koutsodendris, A., Panagiotopoulos, K., Masi, A., Bertini, A., Combourieu-Nebout, N., Francke, A., Kouli, K.,  
1032 Joannin, S., Mercuri, A. M., Peyron, O., Torri, P., Wagner, B., Zanchetta, G., Sinopoli, G., and Donders, T. H.: Pollen-based  
1033 paleoenvironmental and paleoclimatic change at Lake Ohrid (south-eastern Europe) during the past 500 ka, *Biogeosciences*,  
1034 13, 1423–1437, <https://doi.org/10.5194/bg-13-1423-2016>, 2016b.
- 1035 Sanchez Goñi, M. F. and Harrison, S. P.: Millennial-scale climate variability and vegetation changes during the Last Glacial:  
1036 Concepts and terminology, *Quaternary Science Reviews*, 29, 2823–2827, <https://doi.org/10.1016/j.quascirev.2009.11.014>,  
1037 2010.
- 1038 Sanei, H., Grasby, S., and Beauchamp, B.: Latest Permian mercury anomalies, *Geology*, 40, 63–66, 2012.
- 1039 Schlüter, K.: Review: Evaporation of mercury from soils. An integration and synthesis of current knowledge, *Environmental  
1040 Geology*, 39, 249–271, <https://doi.org/10.1007/s002540050005>, 2000.
- 1041 Schneider, L., Cooke, C. A., Stansell, N. D., and Haberle, S. G.: Effects of climate variability on mercury deposition during the  
1042 Older Dryas and Younger Dryas in the Venezuelan Andes, *Journal of Paleolimnology*, 63, 211–224,  
1043 <https://doi.org/10.1007/s10933-020-00111-7>, 2020.
- 1044 Schotsmans, E. M. J., Busacca, G., Lin, S. C., Vasić, M., Lingle, A. M., Veropoulidou, R., Mazzucato, C., Tibbetts, B., Haddow,  
1045 S. D., Somel, M., Toksoy-Köksal, F., Knüsel, C. J., and Milella, M.: New insights on commemoration of the dead through  
1046 mortuary and architectural use of pigments at Neolithic Çatalhöyük, Turkey, *Sci Rep*, 12, 4055, <https://doi.org/10.1038/s41598-022-07284-3>, 2022.
- 1048 Schuster, P. F., Schaefer, K. M., Aiken, G. R., Antweiler, R. C., Dewild, J. F., Gryziec, J. D., Gusmeroli, A., Hugelius, G.,  
1049 Jafarov, E., Krabbenhoft, D. P., Liu, L., Herman-Mercer, N., Mu, C., Roth, D. A., Schaefer, T., Striegl, R. G., Wickland, K. P.,  
1050 and Zhang, T.: Permafrost Stores a Globally Significant Amount of Mercury, *Geophysical Research Letters*, 45, 1463–1471,  
1051 <https://doi.org/10.1002/2017GL075571>, 2018.
- 1052 Schütze, M., Tserendorj, G., Pérez-Rodríguez, M., Rösch, M., and Biester, H.: Prediction of Holocene mercury accumulation  
1053 trends by combining palynological and geochemical records of lake sediments (Black Forest, Germany), *Geosciences  
1054 (Switzerland)*, 8, <https://doi.org/10.3390/geosciences8100358>, 2018.
- 1055 Selin, N. E.: Global biogeochemical cycling of mercury: a review, *Annual Review of Environmental Resources*, 34, 43–63,  
1056 2009.
- 1057 Shakesby, R. A.: Post-wildfire soil erosion in the Mediterranean: Review and future research directions, *Earth-Science  
1058 Reviews*, 105, 71–100, <https://doi.org/10.1016/j.earscirev.2011.01.001>, 2011.



- 1059 Shen, J., Feng, Q., Algeo, T. J., Liu, J., Zhou, C., Wei, W., Liu, J., Them, T. R., Gill, B. C., and Chen, J.: Sedimentary host  
1060 phases of mercury (Hg) and implications for use of Hg as a volcanic proxy, *Earth and Planetary Science Letters*, 543, 116333,  
1061 <https://doi.org/10.1016/j.epsl.2020.116333>, 2020.
- 1062 Sial, A. N., Lacerda, L. D., Ferreira, V. P., Frei, R., Marquillas, R. A., Barbosa, J. A., Gaucher, C., Windmöller, C. C., and  
1063 Pereira, N. S.: Mercury as a proxy for volcanic activity during extreme environmental turnover: The Cretaceous–Paleogene  
1064 transition, *Palaeogeography, Palaeoclimatology, Palaeoecology*, 387, 153–164, <https://doi.org/10.1016/j.palaeo.2013.07.019>,  
1065 2013.
- 1066 Simonsen, M. F., Baccolo, G., Blunier, T., Borunda, A., Delmonte, B., Frei, R., Goldstein, S., Grinsted, A., Kjær, H. A., Sowers,  
1067 T., Svensson, A., Vinther, B., Vladimirova, D., Winckler, G., Winstrup, M., and Vallelonga, P.: East Greenland ice core dust  
1068 record reveals timing of Greenland ice sheet advance and retreat, *Nature Communications*, 10, <https://doi.org/10.1038/s41467-019-12546-2>, 2019.
- 1070 Soerensen, Anne. L., Schartup, A. T., Gustafsson, E., Gustafsson, B. G., Undeman, E., and Björn, E.: Eutrophication Increases  
1071 Phytoplankton Methylmercury Concentrations in a Coastal Sea—A Baltic Sea Case Study, *Environ. Sci. Technol.*, 50, 11787–  
1072 11796, <https://doi.org/10.1021/acs.est.6b02717>, 2016.
- 1073 Stern, G. A., Sanei, H., Roach, P., DeLaronde, J., and Outridge, P. M.: Historical Interrelated Variations of Mercury and Aquatic  
1074 Organic Matter in Lake Sediment Cores from a Subarctic Lake in Yukon, Canada: Further Evidence toward the Algal-Mercury  
1075 Scavenging Hypothesis, *Environ. Sci. Technol.*, 43, 7684–7690, <https://doi.org/10.1021/es902186s>, 2009.
- 1076 Streets, D. G., Horowitz, H. M., Lu, Z., Levin, L., Thackray, C. P., and Sunderland, E. M.: Five hundred years of anthropogenic  
1077 mercury: spatial and temporal release profiles\*, *Environ. Res. Lett.*, 14, 084004, <https://doi.org/10.1088/1748-9326/ab281f>,  
1078 2019.
- 1079 Styllas, M. N., Schimmelpfennig, I., Benedetti, L., Ghilardi, M., Aumaitre, G., Bourlès, D., and Keddadouche, K.: Late-glacial  
1080 and Holocene history of the northeast Mediterranean mountains - New insights from in situ-produced <sup>36</sup>Cl-based cosmic ray  
1081 exposure dating of paleo-glacier deposits on Mount Olympus, Greece, *Quaternary Science Reviews*, 193, 244–265,  
1082 <https://doi.org/10.1016/j.quascirev.2018.06.020>, 2018.
- 1083 Takenaka, C., Shibata, H., Tomiyasu, T., Yasumatsu, S., and Muroo, S.: Effects of forest fires on mercury accumulation in soil  
1084 at the artisanal small-scale gold mining, *Environ Monit Assess*, 193, 699, <https://doi.org/10.1007/s10661-021-09394-3>, 2021.
- 1085 Them, T. R., Jagoe, C. H., Caruthers, A. H., Gill, B. C., Grasby, S. E., Gröcke, D. R., Yin, R., and Owens, J. D.: Terrestrial  
1086 sources as the primary delivery mechanism of mercury to the oceans across the Toarcian Oceanic Anoxic Event (Early  
1087 Jurassic), *Earth and Planetary Science Letters*, 507, 62–72, <https://doi.org/10.1016/j.epsl.2018.11.029>, 2019.
- 1088 Thienemann, M., Masi, A., Kusch, S., Sadori, L., John, S., Francke, A., Wagner, B., and Rethemeyer, J.: Organic geochemical  
1089 and palynological evidence for Holocene natural and anthropogenic environmental change at Lake Dojran  
1090 (Macedonia/Greece), *The Holocene*, 27, 1103–1114, <https://doi.org/10.1177/0959683616683261>, 2017.
- 1091 Tisserand, D., Guédrón, S., Viollier, E., Jézéquel, D., Rigaud, S., Campillo, S., Sarret, G., Charlet, L., and Cossa, D.: Mercury,  
1092 organic matter, iron, and sulfur co-cycling in a ferruginous meromictic lake, *Applied Geochemistry*, 146, 105463,  
1093 <https://doi.org/10.1016/j.apgeochem.2022.105463>, 2022.
- 1094 Tzedakis, P. C., Hooghiemstra, H., and Pälike, H.: The last 1.35 million years at Tenaghi Philippon: revised chronostratigraphy  
1095 and long-term vegetation trends, *Quaternary Science Reviews*, 25, 3416–3430,  
1096 <https://doi.org/10.1016/j.quascirev.2006.09.002>, 2006.
- 1097 Ulfers, A., Zeeden, C., Wagner, B., Krastel, S., Buness, H., and Wonik, T.: Borehole logging and seismic data from Lake Ohrid  
1098 (North Macedonia/Albania) as a basis for age-depth modelling over the last one million years, *Quaternary Science Reviews*,  
1099 276, 107295, <https://doi.org/10.1016/j.quascirev.2021.107295>, 2022.
- 1100 United Nations Environment Programme: Global Mercury Assessment, United Nations, 2018.
- 1101 Van Vliet-Lanoë, B. M. J. and Hallegouët, B.: European permafrost at the LGM and at its maximal extent, in: *Permafrost  
1102 Response on Economic Development, Environmental Security and Natural Resources*, vol. 76, Springer, Dordrecht, 195–213,  
1103 2001.
- 1104 Vandal, G. M., Fitzgerald, W. F., Boutron, C. F., and Candelone, J. P.: Variations in mercury deposition to Antarctica over the  
1105 past 34,000 years, *Nature*, 362, 621–623, <https://doi.org/10.1038/362621a0>, 1993.
- 1106 Vogel, H., Wagner, B., Zanchetta, G., Sulpizio, R., and Rosén, P.: A paleoclimate record with tephrochronological age control  
1107 for the last glacial-interglacial cycle from Lake Ohrid, Albania and Macedonia, *Journal of Paleolimnology*, 44, 295–310,  
1108 <https://doi.org/10.1007/s10933-009-9404-x>, 2010.
- 1109 Wagner, B., Lotter, A. F., Nowaczyk, N., Reed, J. M., Schwab, A., Sulpizio, R., Valsecchi, V., Wessels, M., and Zanchetta, G.:  
1110 A 40,000-year record of environmental change from ancient Lake Ohrid (Albania and Macedonia), *Journal of Paleolimnology*,  
1111 41, 407–430, <https://doi.org/10.1007/s10933-008-9234-2>, 2009.



- 1112 Wagner, B., Vogel, H., Zanchetta, G., and Sulpizio, R.: Environmental change within the Balkan region during the past ca. 50  
1113 ka recorded in the sediments from lakes Prespa and Ohrid, *Biogeosciences*, 7, 3187–3198, [https://doi.org/10.5194/bg-7-3187-](https://doi.org/10.5194/bg-7-3187-2010)  
1114 2010, 2010.
- 1115 Wagner, B., Aufgebauer, A., Vogel, H., Zanchetta, G., Sulpizio, R., and Damaschke, M.: Late Pleistocene and Holocene  
1116 contourite drift in Lake Prespa (Albania/F.Y.R. of Macedonia/Greece), *Quaternary International*, 274, 112–121,  
1117 <https://doi.org/10.1016/j.quaint.2012.02.016>, 2012.
- 1118 Wagner, B., Leng, M. J., Wilke, T., Böhm, A., Panagiotopoulos, K., Vogel, H., Lacey, J. H., Zanchetta, G., and Sulpizio, R.:  
1119 Distinct lake level lowstand in Lake Prespa (SE Europe) at the time of the 74 (75) ka Toba eruption, *Climate of the Past*, 10,  
1120 261–267, <https://doi.org/10.5194/cp-10-261-2014>, 2014.
- 1121 Wagner, B., Vogel, H., Francke, A., Friedrich, T., Donders, T., Lacey, J. H., Leng, M. J., Regattieri, E., Sadori, L., Wilke, T.,  
1122 Zanchetta, G., Albrecht, C., Bertini, A., Combourieu-Nebout, N., Cvetkoska, A., Giaccio, B., Grazhdani, A., Hauffe, T.,  
1123 Holtvoeth, J., Joannin, S., Jovanovska, E., Just, J., Kouli, K., Kousis, I., Koutsodendris, A., Krastel, S., Lagos, M., Leicher, N.,  
1124 Levkov, Z., Lindhorst, K., Masi, A., Melles, M., Mercuri, A. M., Nomade, S., Nowaczyk, N., Panagiotopoulos, K., Peyron, O.,  
1125 Reed, J. M., Sagnotti, L., Sinopoli, G., Stelbrink, B., Sulpizio, R., Timmermann, A., Tofilovska, S., Torri, P., Wagner-Cremer, F.,  
1126 Wonik, T., and Zhang, X.: Mediterranean winter rainfall in phase with African monsoons during the past 1.36 million years,  
1127 *Nature*, 573, 256–260, <https://doi.org/10.1038/s41586-019-1529-0>, 2019.
- 1128 Wagner, B., Tauber, P., Francke, A., Leicher, N., Binnie, S. A., Cvetkoska, A., Jovanovska, E., Just, J., Lacey, J. H., Levkov, Z.,  
1129 Lindhorst, K., Kouli, K., Krastel, S., Pana-giotopoulos, K., Ulfers, A., Zaova, D., Donders, T. H., Grazhdani, A., Koutsodendris,  
1130 A., Leng, M. J., Sadori, L., Scheinert, M., Vogel, H., Wonik, T., Zanchetta, G., and Wilke, T.: The geodynamic and limnological  
1131 evolution of Balkan Lake Ohrid, possibly the oldest extant lake in Europe, *Boreas*, bor.12601,  
1132 <https://doi.org/10.1111/bor.12601>, 2022.
- 1133 Wang, F., Outridge, P. M., Feng, X., Meng, B., Heimbürger-Boavida, L. E., and Mason, R. P.: How closely do mercury trends in  
1134 fish and other aquatic wildlife track those in the atmosphere? – Implications for evaluating the effectiveness of the Minamata  
1135 Convention, *Science of the Total Environment*, 674, 58–70, <https://doi.org/10.1016/j.scitotenv.2019.04.101>, 2019.
- 1136 Warriar, A. K., Pednekar, H., Mahesh, B. S., Mohan, R., and Gazi, S.: Sediment grain size and surface textural observations of  
1137 quartz grains in late quaternary lacustrine sediments from Schirmacher Oasis, East Antarctica: Paleoenvironmental  
1138 significance, *Polar Science*, 10, 89–100, <https://doi.org/10.1016/j.polar.2015.12.005>, 2016.
- 1139 Watanabe, T., Naraoka, H., Nishimura, M., and Kawai, T.: Biological and environmental changes in Lake Baikal during the late  
1140 Quaternary inferred from carbon, nitrogen and sulfur isotopes, *Earth and Planetary Science Letters*, 222, 285–299,  
1141 <https://doi.org/10.1016/j.epsl.2004.02.009>, 2004.
- 1142 Woodward, J. C., Hamlin, R. H. B., Macklin, M. G., Hughes, P. D., and Lewin, J.: Glacial activity and catchment dynamics in  
1143 northwest Greece: Long-term river behaviour and the slackwater sediment record for the last glacial to interglacial transition,  
1144 *Geomorphology*, 101, 44–67, <https://doi.org/10.1016/j.geomorph.2008.05.018>, 2008.
- 1145 Zaferani, S. and Biester, H.: Mercury Accumulation in Marine Sediments – A Comparison of an Upwelling Area and Two Large  
1146 River Mouths, *Front. Mar. Sci.*, 8, 732720, <https://doi.org/10.3389/fmars.2021.732720>, 2021.
- 1147 Zanchetta, G., Giaccio, B., Bini, M., and Sarti, L.: Tephrostratigraphy of Grotta del Cavallo, Southern Italy: Insights on the  
1148 chronology of Middle to Upper Palaeolithic transition in the Mediterranean, *Quaternary Science Reviews*, 182, 65–77,  
1149 <https://doi.org/10.1016/j.quascirev.2017.12.014>, 2018.
- 1150 Zhang, Q., Huang, J., Wang, F., Mark, L., Xu, J., Armstrong, D., Li, C., Zhang, Y., and Kang, S.: Mercury distribution and  
1151 deposition in glacier snow over Western China, *Environmental Science and Technology*, 46, 5404–5413,  
1152 <https://doi.org/10.1021/es300166x>, 2012.
- 1153